Ceramics International 51 (2025) 32808–32820

Contents lists available at ScienceDirect

Ceramics International

journal homepage: www.elsevier.com/locate/ceramint

Study of Mg doping on the zirconium and lanthanide sites of $Ln_2Zr_2O_7$ (*Ln* = Sm, Gd) pyrochlores

N.V. Lyskov [a], I.V. Kolbanev [b], A.B. Borunova [b], G.A. Vorobieva [b], J.C.C. Abrantes [c], E. Gomes [c], N.A. Danilov [d,e], D.A. Medvedev [d,e], A.V. Shlyakhtina [b,*]

[a] Federal Research Center of Problems of Chemical Physics and Medical Chemistry RAS, Chernogolovka, Russia
[b] N.N. Semenov Federal Research Center for Chemical Physics RAS, Moscow, Russia
[c] proMetheus, Instituto Politécnico de Viana do Castelo, 4900-348 Viana do Castelo, Viana do Castelo, Portugal
[d] Institute of High Temperature Electrochemistry, Ural Branch, RAS, Russia
[e] Ural Federal University, First President of Russia B.N. Yeltsin, Russia

ARTICLE INFO

Handling Editor: Dr P. Vincenzini

Keywords:
REE zirconates
Pyrochlores
Fluorites
Oxygen-ion conductivity
Proton conductivity

ABSTRACT

$Ln_2Zr_2O_7$ (*Ln* = Sm, Gd) zirconate solid solutions doped with Mg on the *Ln* and Zr sites have been prepared via mechanical activation of oxide mixtures, followed by heat treatment of green compacts at 1500 and 1600 °C for 4 h. The ceramics prepared at 1600 °C have been characterized by X-ray diffraction and scanning electron microscopy. Their electrical conductivity has been determined in dry and wet air using impedance spectroscopy, and the total conductivity of the best samples has been measured from 700 to 1000 °C in a wide range of oxygen partial pressures. The conductivity data obtained in dry and wet air for the samarium zirconate-based solid solutions doped with Mg on the Zr site demonstrate that raising the Mg content on the Zr site in the $Sm_2Zr_{2-x}Mg_xO_{7-\delta}$ (x = 0, 0.05, 0.1, 0.2) pyrochlore series leads to a decrease in the total conductivity of the materials. However, the $Sm_2Zr_{2-x}Mg_xO_{7-\delta}$ (x = 0.05, 0.1) materials have a proton component of conductivity in the range of 300–600 °C, which also decreases with increasing Mg content. Among the samarium zirconates studied here, high proton conductivity (1×10^{-4} S/cm at 500°C) is offered by the $Sm_2Zr_{1.95}Mg_{0.05}O_{7-\delta}$ solid solution. $Sm_{1.9}Mg_{0.1}Zr_2O_{7-\delta}$, containing Mg on the Sm site, has the highest oxygen ion conductivity: 5×10^{-3} S/cm at 750°C. The total conductivity of the $Gd_2Zr_{2-x}Mg_xO_{7-\delta}$ (x = 0, 0.05, 0.1, 0.2) series also decreases with increasing Mg content, and no proton conduction has been detected in these zirconates. Mg doping of $Gd_2Zr_2O_7$ on the Zr site reduces the total conductivity of the material, whereas Mg doping on the Gd site ($Gd_{1.9}Mg_{0.1}Zr_2O_{7-\delta}$) raises it to 7.5×10^{-3} S/cm at 750 °C.

1. Introduction

It is known that, for practical applications, the oxygen ion conductivity of solid oxide fuel cell (SOFC) electrolytes should be in the range 8.4×10^{-3} to 7.4×10^{-2} S/cm at 700 °C [1]. This high level of oxygen ion conductivity is offered by 8YSZ (8 mol% Y_2O_3-stabilized ZrO_2) [2,3], gadolinium-doped ceria GDC ($Ce_{0.9}Gd_{0.1}O_{1.95}$) [4,5] and scandia-stabilized zirconia (ScSZ) [6–10] solid electrolytes. The last one is known to undergo a phase transition from the high-conductive cubic phase to a low-conductive tetragonal phase during cooling or aging at 1250–1550°C [6], but Ce doping of scandia-stabilized zirconia, e.g. in the case of the composition $(Sc_2O_3)_{0.08}(CeO_2)_{0.01}(ZrO_2)_{0.91}$, was shown to stabilize its cubic phase in a wide temperature range [8–10].

Raising the Ln_2O_3 content of the Ln_2O_3-ZrO_2 (*Ln* = La - Gd) systems to 33.3 mol. % leads to the formation of pyrochlore-structured compounds $Ln_2Zr_2O_7$. In the pyrochlore $Ln_2Zr_2O_7$ series, the compounds near the pyrochlore–fluorite morphotropic phase boundary, i.e. the $Ln_2Zr_2O_7$ (*Ln* = Sm, Eu, Gd) compounds, are known to have the highest oxygen ion conductivity [11–14]. The material of most practical interest is $Gd_2Zr_2O_7$, whose conductivity at 700 °C is 1×10^{-3} S/cm, and the fact that gadolinium has only one oxidation state (Gd^{3+}) is favorable for the stability of this material in a reducing atmosphere and in the working temperature range of fuel cells (500–800 °C). Thus, to reach conductivity optimal for practical application ($8.4 \times 10^{-3} - 7.4 \times 10^{-2}$ S/cm at 700°C [1]), a dopant capable of raising the conductivity of $Gd_2Zr_2O_7$ by an order of magnitude should be found.

* Corresponding author.
E-mail addresses: annashl@inbox.ru, annash@chph.ras.ru (A.V. Shlyakhtina).

https://doi.org/10.1016/j.ceramint.2025.05.015
Received 16 October 2024; Received in revised form 4 March 2025; Accepted 4 May 2025
Available online 5 May 2025

Since $Gd_2Zr_2O_7$ is the most attractive material for doping because its own oxygen ion conductivity is high, in many studies both iso- and aliovalent doping on the Gd and Zr sites was used to raise its conductivity [15–18]. For example, Diaz-Guillen et al. [15,16] studied electrical properties of the $Gd_{2-y}La_yZr_2O_7$ ($0 \le y \le 1$) series. The synthesis temperature was 1200 [15] and 1500 °C [16]. In the lower temperature series, the highest conductivity was offered by the $Gd_{2-y}La_yZr_2O_7$ ($y = 0.4$) solid solution: 7×10^{-4} S/cm at 700 °C [15]. When the synthesis temperature was raised to 1500 °C, the highest conductivity in air was obtained in the case of $Gd_{2-y}La_yZr_2O_7$ ($y = 0.8$): 4×10^{-3} S/cm at 700°C. In our opinion, interesting results were reported by Xia et al. [17], who studied the conductivity of $Gd_2Zr_{2-x}Nb_xO_7$ ($0 \le x \le 0.4$). The highest electrical conductivity was observed for $Gd_2Zr_{2-x}Nb_xO_{7.1}$ ($x = 0.1$). The authors believe that this ceramic has proton conductivity because its conductivity in H_2 is slightly higher than in air. It is worth noting that none of the cations in this solid solution have pronounced basic properties and, accordingly, all of them have low activity upon proton dissolution in the lattice, unlike in the case of, e.g., Ca^{2+}-doped $La_2Zr_2O_7$ [19].

Doping of $Gd_2Zr_2O_7$ with Ca and Sr divalent cations has been the subject of the most intensive research effort [20–22], but no significant increase in conductivity was ensured. For example, the oxygen ion conductivity of $Gd_{2-x}Ca_xZr_2O_{7-\delta}$ ($x = 0.1$) was determined to be 1.2×10^{-3} S/cm at 700 °C [22]. In a number of studies, the conductivity of the Ca-doped material was even observed to decrease with increasing Ca concentration. It is important to emphasize that, in the case of $Gd_{2-x}Ca_xZr_2O_{7-x/2}$ ($x = 0.1$), only its grain-boundary conductivity responded to changes in ambient humidity, and this was shown to be due to a perovskite $CaZrO_3$-based proton-conducting impurity phase formed on grain boundaries [21,22].

Shlyakhtina et al. [23] and Liu et al. [24] reported doping with beryllium and molybdenum on the Zr site, which led to a decrease in oxygen ion conductivity. Xia et al. [17] and Anokhina et al. [25,26] doped with Nb and Li on the Zr site observed an increase in oxygen ion conductivity at degrees of substitution of up to $x = 0.1$, but the conductivity dropped at higher degrees of substitution [17,26]. The best results were obtained in the case of $Gd_{1.7}Li_{0.3}Zr_2O_{6.7}$ [25], with a high degree of Li substitution on the Gd site: its oxygen ion conductivity ($\sim 8 \times 10^{-3}$ S/cm at 700 °C) was an order of magnitude higher than that of undoped $Gd_2Zr_2O_7$.

Comparing the dependence of total conductivity on oxygen partial pressure for ceramics doped on the Zr site, we note a considerable region of purely oxygen ion conductivity, without a hole contribution (at high oxygen partial pressures) or an electron contribution (at low oxygen partial pressures) in the case of ceramics doped on the Zr site with Li (below 750 °C), Be (below 900 °C), or Mo (below 800 °C) [20,22,25]. At the same time, above 600 °C, the most promising solid solution $Gd_{1.7}Li_{0.3}Zr_2O_{6.7}$ has hole and electron conductivity at high and low oxygen partial pressures, respectively, with a marked decrease in the region of purely ionic conductivity [25]. In the case of Ca doping of $Gd_2Zr_2O_7$, the $Gd_{2-x}CaZr_2O_{7-x/2}$ ($x = 0.1$) solid solution had no hole conduction in a wide temperature range, up to 950 °C, but at low oxygen partial pressures the electron contribution markedly reduced the oxygen pressure range where ionic conduction prevailed (from 10^{-20} Pa at 700 °C to 10^{-12} Pa at 950 °C) [22].

As mentioned above, Ca-doped $Gd_2Zr_2O_7$-based solid solutions demonstrate bulk oxygen ion conduction over the entire temperature range measured. This distinguishes them from pyrochlore Ca-doped $Sm_2Zr_2O_7$-based solid solutions, which were shown to have proton contributions to their bulk and grain-boundary conductivity below 600 °C [22,27]. Note that, above 700 °C, the oxygen ion conductivity of $Sm_{2-x}Ca_xZr_2O_{7-x/2}$ ($x = 0.1$) (2.5×10^{-3} S/cm at 700 °C) slightly exceeds that of $Gd_{2-x}Ca_xZr_2O_{7-x/2}$ ($x = 0.1$), which is due to the more disordered structure of the latter. The oxygen ion conductivity data reported by Xia et al. [28] for $Sm_{2-x}Ca_xZr_2O_{7-x/2}$ agree with later results [21,22].

Along with high conductivity, an important point for practical application is the absence of hole conduction in SOFCs at high oxygen partial pressures and in air [29]. As shown earlier [22], $Gd_{2-x}Ca_xZr_2O_{7-x/2}$ ($x = 0.1$) has no hole conductivity at least up to 800 °C, like the $Sm_{2-x}Ca_xZr_2O_{7-x/2}$ ($x = 0.05$) solid solution [22], but the latter has a very narrow purely ionic conductivity region.

There is very limited information about magnesium doping of the $Ln_2Zr_2O_7$ (Ln = Sm, Gd) pyrochlores. One exception is a report by Qu et al. [30], who related the observed variation in the thermal expansion coefficient of $Sm_2Zr_2O_7$-based solid solutions to defect chemistry. Their results demonstrate that, at low doping levels, Mg occupies interstitial sites, whereas at higher doping levels Mg cations begin to occupy the Sm site, producing oxygen vacancies. These processes can be represented by the following Kröger–Vink equations:

$$MgO + V_O^{\bullet\bullet} \rightarrow Mg_i^{\bullet\bullet} + O_O^{\times} \quad (1)$$

$$2MgO \xrightarrow{Ln_2O_3} 2Mg'_{Ln} + 2O_O^{\times} + V_O^{\bullet\bullet} \quad (2)$$

Xiong et al. [31] co-doped $Sm_2Zr_2O_7$ with Dy and Mg on the Sm site ($(SmDy_{1-x}Mg_x)Zr_2O_{7-x/2}$ ($0 \le x \le 0.20$)), but the oxygen ion conductivity of the resultant material was just $\sim 1 \times 10^{-3}$ S/cm at 700 °C, whereas the conductivity of the $(GdSm_{1-x}Mg_x)Zr_2O_{7-x/2}$ ($x = 0.15$) solid solution was four times higher [32].

Shimura et al. [33] studied the proton conductivity of $Ln_2Zr_2O_7$ (Ln = La, Nd, Sm, Gd, Er) based rare-earth oxides with the pyrochlore structure and showed that, in a hydrogen atmosphere above 600 °C, the conductivity of $Ln_2Zr_{1.8}Y_{0.2}O_{7-\delta}$ (Ln = La, Nd, Sm, Gd), doped with yttrium on the Zr site, was comparable to that of perovskites. The $Ln_2Zr_{1.8}Y_{0.2}O_{7-\delta}$ (Ln = La, Nd, Sm, Gd) materials were shown to be pure proton conductors in hydrogen, whereas in an oxidizing atmosphere they had oxygen ion conductivity with a transport number under unity, except for $Gd_2Zr_{1.8}Y_{0.2}O_{7-\delta}$.

A number of detailed studies have been concerned with how substitutions of Y and Mg, Ca, Sr, and Ba alkaline-earth cations on the La and Zr sites in the pyrochlore structure of $La_2Zr_2O_7$ influence its proton conductivity [19,34,35]. The proton conductivity of the materials acceptor-doped on the La site was shown to be about three times that in the case of Zr-site substitution [19].

It is worth noting that we have found no data on Zr-site doping of $Ln_2Zr_2O_7$ (Ln = Sm, Gd) with Mg, even though it is Zr-site doping with Y^{3+} which favours proton conduction in rare-earth pyrochlores [33].

The pyrochlore unit cell contains 88 atoms and has a rather complex arrangement of atoms. Doping with small cations ($\Delta_1 = r\left(Sm_{VIII}{}^{3+}\right) - r\left(Mg_{VIII}{}^{2+}\right) = 0.189$ Å and $\Delta_2 = r\left(Gd_{VIII}{}^{3+}\right) - r\left(Mg_{VIII}{}^{2+}\right) = 0.163$ Å) would be expected to be more successful than that with large cations: calcium and strontium [31]. A smaller dopant size can ensure a more uniform dopant distribution over the structure [36]. Although Ca and Sr are known to have the greatest tendency toward hydration among divalent dopants, whereas Mg is less susceptible to hydration [34].

The purpose of this work was to study the conductivity of $Ln_2(Zr_{2-x}Mg_x)O_{7-\delta}$ (Ln = Sm, Gd, Dy; $x = 0$, 0.05, 0.1, 0.2) solid solutions, containing Mg on the Zr site, and compare the results to the conductivity of $Ln_{2-x}Mg_xZr_2O_{7-\delta}$ (Ln = Sm, Gd; $x = 0.1$), containing Mg on the lanthanide site.

2. Experimental part

$Ln_2(Zr_{2-x}Mg_x)O_{7-\delta}$ (Ln = Sm, Gd; x = 0, 0.05, 0.1, 0.2) and $Ln_{2-x}Mg_xZr_2O_{7-\delta}$ (Ln = Sm, Gd; x = 0, 0.1, 0.3) were synthesized by reacting appropriate oxide mixtures (Ln_2O_3 (Ln = Sm, Gd) + ZrO_2 + MgO) after mechanical activation in a SPEX8000 ball mill. Initial reagents: Gd_2O_3 (99.99 % purity, Aldrich Chem Company, Inc.), Sm_2O_3 (99.99 %, manufactured by OOO Lankhit, Russia), ZrO_2 (99 %, Aldrich Chem Company, Inc.), MgO (99.99 %, Aldrich Chem Company, Inc.).

The parameters of SPEX8000 ball mill are presented in Ref. [22]. The

Ln_2O_3 (Ln = Sm, Gd) starting powders were annealed at 1000 °C for 2 h and then placed in a desiccator after cooling to 850 °C. After the milling, the mixtures were pressed at 680 MPa and then fired at 1500 or 1600 °C for 4 h in air. In addition, we synthesized $(Dy_2(Zr_{2-x}Mg_x)O_{7-\delta}$ ($x = 0.1$) fluorite by a similar procedure in order to compare its properties to those of $Ln_2(Zr_{2-x}Mg_x)O_{7-\delta}$ (Ln = Sm, Gd, $x = 0.1$). The Dy precursor used was Dy_2O_3 (DiO-I, TU 48-4-193-72).

The density of the resultant 1600 °C samples was determined by measuring their mass and dimensions and ranged from 87.4 to 99 % of their X-ray density. In some cases, the density of the samples was determined by hydrostatic weighing in toluene. Characteristics of the compounds and solid solutions under investigation presented in Table 1. All of the synthesized solid solutions were characterized by X-ray diffraction (XRD) on a DRON-3M (filtered Cuk_α radiation, step scan mode with a step of 0.1°, angular range 2θ = 10–75°).

The microstructure of the sintered ceramics was examined using scanning electron microscopy (JEOL JSM-6390LA). Using the SEM method, we analysed the grain size distribution and porosity of the ceramics on the polished and thermal etched or fresh surfaces.

Thermogravimetric analysis was performed by using the NETZSCH STA 449C system (30–1000 °C, heating rate of 10 K/min, Al_2O_3 plate) in O_2 atmosphere. A detailed description of the experiment can be found in Ref. [37].

The conductivity of the sintered ceramic materials was measured by both 2-probe AC and 4-probe DC methods. Disk-shaped polycrystalline samples (diameter ~ 9 mm and thickness 2–3 mm) were used for measurements by the 2-probe AC method. Contacts to the sample faces were made by firing ChemPur C3605 paste, containing colloidal platinum, at 950 °C, 0.5 h. The conductivity of $Sm_2(Zr_{2-x}Mg_x)O_{7-\delta}$ ($x = 0$, 0.05, 0.1, 0.2) (SmZrMgO system), $Gd_2(Zr_{2-x}Mg_x)O_{7-\delta}$ ($x = 0$, 0.05, 0.1, 0.2) (GdZrMgO system), $Dy_2(Zr_{2-x}Mg_x)O_{7-\delta}$ (x = 0.1) and $Ln_{2-x}Mg_xZr_2O_{7-\delta}$ (Ln = Sm, Gd; x = 0.1, 0.3) was characterized by impedance spectroscopy in dry and wet air. Electrical conductivity measurements of the samples were performed on cooling regime using a P-40X potentiostat/galvanostat combined with frequency response analyzer module (Elins Ltd, Russia) over the frequency range of 0.1 Hz–500 kHz at signal amplitude of 150 mV in the temperature range of 100–900 °C. Dry atmosphere was created by passing air through a KOH and wet atmosphere - through a water saturator held at 20 °C, which ensured constant humidity of about 0.023 atm. (2.3 % H_2O). Air flow rate was 130 ml/min. To get stable state (water vapor pressure) before conductivity measurement, the sample was kept at each temperature for 40 min. In fitting impedance measurement results and calculating total conductivity, we used a classic model based on an equivalent electrical circuit that describes ion transport in ceramic solid electrolytes in terms of a combination of bulk and grain boundary resistances (Bauerle model) [38].

The 4-probe DC measurements were carried out using a microprocessor regulator Zirconia-M (Zirconia, Russia). A bar-shaped sample was cut from the sintered ceramic of the composition $Sm_2(Zr_{2-x}Mg_x)O_{7-\delta}$ (x = 0.05). Four platinum wires were wound on the sample. A platinum paste was deposited on the contact points of platinum wires with the sample. After that, firing was performed at 1100 °C for 1 h. Measurements were carried out in heating mode in the temperature range of 500–900 °C in oxidizing (dry and wet air) and reducing (wet nitrogen) atmospheres at different humidities. Soaking times were 5 h at 500 °C and 3 h at 600, 700, 800 and 900 °C. The dry air ($pH_2O = 1{\cdot}10^{-4}$ atm., where pH_2O is the water vapor partial pressure) was obtained by passing air through a zeolite column, whereas the wet air and wet nitrogen (pH_2O = 0.03 atm.) were obtained by passing gases through a water bubbler heated to 25 °C.

Electrical characterization of $Ln_{2-x}Mg_xZr_2O_{7-\delta}$ (Ln = Sm, Gd; x = 0.1) was carried out also by impedance spectroscopy in the frequency range of 20 Hz to 1 MHz, with a signal amplitude of 200 mV, using a Hewlett-Packard 4284A precision LCR bridge, as a function of the oxygen partial pressure, during reoxidation, after reduction with a mixture of 95 % N_2 and 5 % H_2, between 700 and 950 °C.

The synthesis and measurements scheme is shown in Fig. 1.

3. Results and discussion

3.1. XRD characterization of $Ln_2Zr_2O_7$ (Ln = Sm, Gd) doped on the Ln and Zr sites

Fig. S1 shows XRD patterns of samarium zirconate-based solid solutions prepared by firing at 1500 °C for 4 h and containing Mg on the Zr site ($Sm_2Zr_{2-x}Mg_xO_{7-\delta}$ (x = 0.05, 0.1, 0.2)) (scans 1–3). Also shown in Fig. 1a are XRD patterns of gadolinium zirconate-based solid solutions containing Mg on the Zr site ($Gd_2Zr_{2-x}Mg_xO_{7-\delta}$ (x = 0.1, 0.2)) (scans 4, 5) and the XRD pattern of $Dy_2Zr_{1.9}Mg_{0.1}O_{7-\delta}$ (scan 6). The intensity of pyrochlore superstructure reflections is seen to decrease with decreasing Ln ionic radius. Almost all of the solid solutions, synthesized at 1500 °C, are phase-pure.

Fig. 2a, scans 1–4, presents XRD data for the $Sm_2Zr_{2-x}Mg_xO_{7-\delta}$ (x = 0, 0.05, 0.1, 0.2) solid solutions prepared by firing at a higher temperature, 1600 °C, for 4 h. In the case of $Sm_2Zr_{2-x}Mg_xO_{7-\delta}$ (x = 0.2), it is

Table 1
Synthesis conditions, density, and average grain size of the materials prepared at 1500 and 1600 °C.

Sample no.	Nominal composition	Synthesis conditions	Geometric density, g/cm^3	Relative geometric density, %	Hydrostatic density (weighing in toluene), g/cm^3	Relative hydrostatic density, %	Average grain size, μm
1	$Sm_2Zr_{1.95}Mg_{0.05}O_{7-\delta}$	1500°C, 4 h	5.81				
2	$Sm_2Zr_{1.9}Mg_{0.1}O_{7-\delta}$	1500°C, 4 h	5.69				
3	$Sm_2Zr_{1.8}Mg_{0.2}O_{7-\delta}$	1500°C, 4 h	5.70				
4	$Gd_2Zr_{1.9}Mg_{0.1}O_{7-\delta}$	1500°C, 4 h	5.40				
5	$Gd_2Zr_{1.8}Mg_{0.2}O_{7-\delta}$	1500°C, 4 h	5.23				
6	$Dy_2Zr_{1.9}Mg_{0.1}O_{7-\delta}$	1500°C, 4 h	5.74				
7	$Sm_2Zr_2O_7$	1600°C, 10 h	5.86	87.4			1.72
8	$Sm_2Zr_{1.95}Mg_{0.05}O_{7-\delta}$	1600°C, 4 h	6.12	92.67	6.31 ± 0.01	95.5	0.94
9	$Sm_2Zr_{1.9}Mg_{0.1}O_{7-\delta}$	1600°C, 4 h	6.08	92.83	6.25 ± 0.01	95.4	1.37
10	$Sm_2Zr_{1.8}Mg_{0.2}O_{7-\delta}$	1600°C, 4 h	6.04	94			1.20
11	$Sm_{1.9}Mg_{0.1}Zr_2O_{7-\delta}$	1600°C, 4 h	6.52	98.96			1.86
12	$Sm_{1.7}Mg_{0.3}Zr_2O_{7-\delta}$	1500°C, 3 h	6.12	97			–
13	$Gd_2Zr_2O_7$	1450°C, 4ч +1600°C, 4 h	6.24	89.74			2.66
14	$Gd_2Zr_{1.95}Mg_{0.05}O_{7-\delta}$	1600°C, 4 h	5.70	82.93	5.92 ± 0.01	86.13	–
15	$Gd_2Zr_{1.9}Mg_{0.1}O_{7-\delta}$	1600°C, 4 h	5.58	81.78			0.90
16	$Gd_2Zr_{1.8}Mg_{0.2}O_{7-\delta}$	1600°C, 4 h	5.77	86.07	5.97 ± 0.01		1.28
17	$Gd_{1.9}Mg_{0.1}Zr_2O_{7-\delta}$	1600°C, 4 h	6.78	99.3			3.42
18	$Dy_2Zr_{1.9}Mg_{0.1}O_{7-\delta}$	1600°C, 4 h	6.09	85.69			1.72

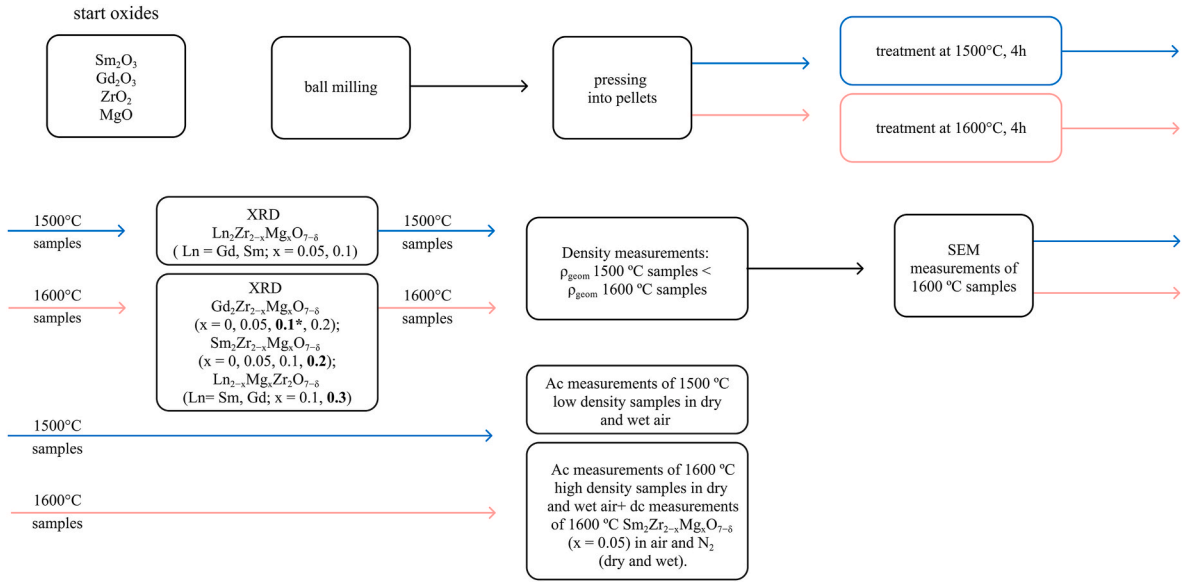

Fig. 1. The synthesis process and measurements scheme. * - Multiphase materials are highlighted in bold.

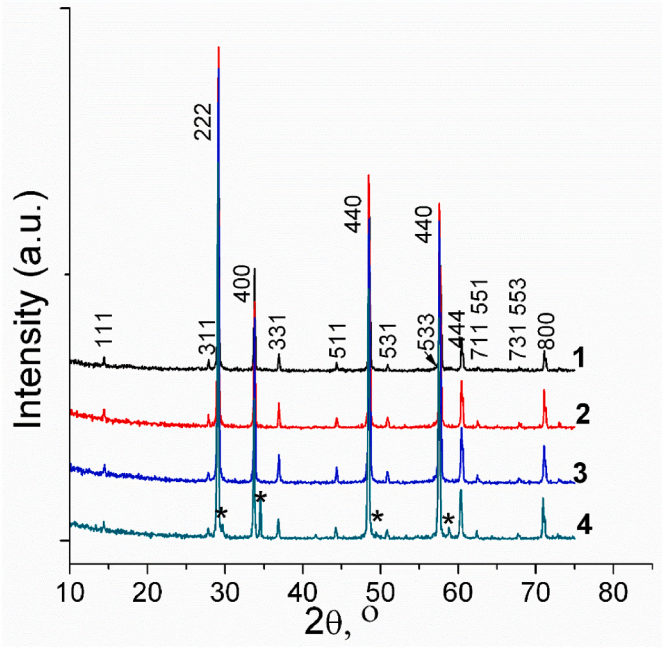

Fig. 2a. XRD of the $Sm_2Zr_{2-x}Mg_xO_{7-\delta}$ (x = 0, 0.05, 0.1, 0.2) samples, synthesized at 1600 °C, 4 h:
(1) $Sm_2Zr_2O_7$; (2) $Sm_2Zr_{1.95}Mg_{0.05}O_{7-\delta}$; (3) $Sm_2Zr_{1.9}Mg_{0.1}O_{7-\delta}$; (4) $Sm_2Zr_{1.8}Mg_{0.2}O_{7-\delta}$ (the impurity phase is marked with asterisks).

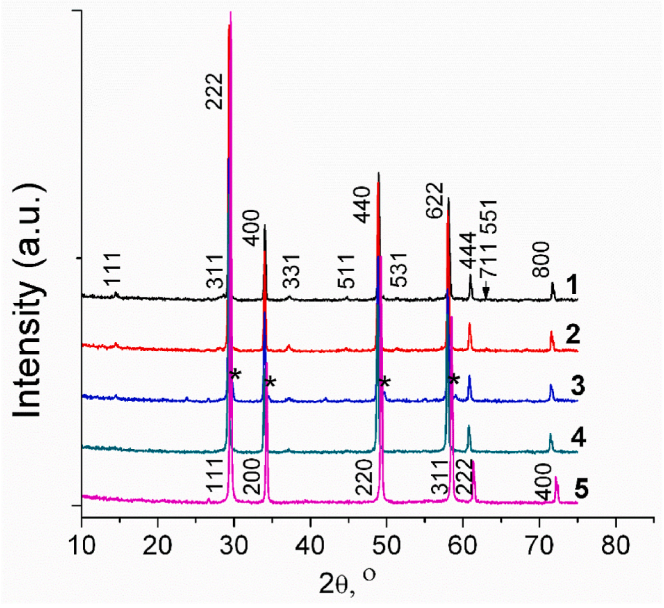

Fig. 2b. XRD of the $Gd_2Zr_{2-x}Mg_xO_{7-\delta}$ (x = 0, 0.05, 0.1, 0.2) samples, synthesized at 1600 °C, 4 h:
(1) $Gd_2Zr_2O_7$; (2) $Gd_2Zr_{1.95}Mg_{0.05}O_{7-\delta}$; (3) $Gd_2Zr_{1.9}Mg_{0.1}O_{7-\delta}$ (the impurity phase is marked with asterisks); (4) $Gd_2Zr_{1.8}Mg_{0.2}O_{7-\delta}$; (5) $Dy_2Zr_{1.9}Mg_{0.1}O_{7-\delta}$.

worth noting the presence of the impurity ZrO_2 fluorite phase (ICDD PDF 37-31) (Fig. 2a, scan 4), with an increased parameter due to doping with Sm (this phase is marked with asterisks in Fig. 2a). Thus, when the zirconium sublattice of $Sm_2Zr_2O_7$ is doped with Mg, the homogeneity region of the pyrochlore is within $0 < x \leq 0.1$.

Fig. 2b presents XRD data for the $Gd_2Zr_{2-x}Mg_xO_{7-\delta}$ (x = 0, 0.05, 0.1, 0.2) series (Fig. 2b, scans 1–4), and $Dy_2Zr_{1.9}Mg_{0.1}O_{7-\delta}$ solid solution (Fig. 2b, scan 5). It is worth noting the formation of a fluorite impurity phase at lower dopant concentrations in comparison with the samarium system (x = 0.1). The formation of a ZrO_2-based fluorite solid solution with an increased parameter due to doping with Gd is observed for $Gd_2Zr_{1.9}Mg_{0.1}O_{7-\delta}$ (Fig. 2b, scan 3). It is remarkable that the solid solution having an even higher dopant concentration, $Gd_2Zr_{1.8}Mg_{0.2}O_{7-\delta}$ (x = 0.2), turned out to be single-phase. We believe that the $Gd_2Zr_{1.9}Mg_{0.1}O_{7-\delta}$ material was obtained in a nonequilibrium state, but, as shown below, the ZrO_2-based fluorite impurity phase had no significant effect on the conductivity of the ceramic (Fig. 7, scans 2, 3). Doping with Mg on the Zr site reduced conductivity in the GdZrMgO system, in spite of the increase in lattice parameter of the single-phase $Gd_2Zr_{2-x}Mg_xO_{7-\delta}$ (x = 0, 0.05, 0.2) materials (Fig. 7, scans 1, 3, 6).

The peaks in the XRD pattern of $Dy_2Zr_{1.9}Mg_{0.1}O_{7-\delta}$ are shifted to larger angles (Fig. 2b, scan 5), indicating that it has a smaller unit-cell parameter in comparison with the gadolinium zirconates $Gd_2Zr_{2-x}Mg_xO_{7-\delta}$ (x = 0, 0.05, 0.1, 0.2). Thus, when the zirconium sublattice of $Sm_2Zr_2O_7$ is doped with Mg, the homogeneity region of the pyrochlore is within $0 < x \leq 0.1$, and when similarly doped with

$Gd_2Zr_2O_7$, it is smaller ($0 < x \leq 0.05$).

Fig. 3 shows the unit-cell parameter and volume as functions of Mg content for the Mg-doped gadolinium and samarium zirconates, including the $Ln_2Zr_2O_7$ (Ln = Sm, Gd) stoichiometric compositions, synthesized at 1600 °C, for 4 h. The data are presented for two zirconate series. Curves 1 in Fig. 3a and b represent the composition dependences of the unit-cell parameter and volume for the gadolinium zirconates doped with Mg on the Zr site $Gd_2Zr_{2-x}Mg_xO_{7-\delta}$ ($x = 0$, 0.05, 0.1, 0.2), and curves 1 in Fig. 3c and d represent such data for the $Sm_2Zr_{2-x}Mg_xO_{7-\delta}$ ($x = 0$, 0.05, 0.1) series. Curves 2 represent data for the $Ln_{2-x}Mg_xZr_2O_{7-\delta}$ (Ln = Sm, Gd; $x = 0$, 0.1) solid solutions, doped with Mg on the lanthanide site. It is more adequate to compare the data for the Sm-containing $Sm_2Zr_{2-x}Mg_xO_{7-\delta}$ ($x = 0$, 0.05, 0.1) samples because they are single-phase.

Curves 1 and 2 in Fig. 3c demonstrate that the unit-cell parameter of $Sm_{1.9}Mg_{0.1}Zr_2O_{7-\delta}$ is smaller than that of $Sm_2Zr_{1.9}Mg_{0.1}O_{7-\delta}$, in accordance with the ionic radii of their constituent cations. Mg^{2+} and Zr^{4+} have the same six-coordinate ionic radius, 0.72 Å [39], so Mg doping on the Zr site would be expected to cause no changes in unit-cell parameter. However, we observe an increase in unit-cell parameter and volume with increasing Mg content on the Zr site. Similar behavior was reported by Vendrell et al. [40], who studied the $Nd_2Zr_{2-x}Mg_xO_{7-\delta}$ ($x = 0.0$, 0.005, 0.01, 0.02) solid solution series. Therefore, Mg^{2+} incorporation into the Zr sublattice leads to the formation of oxygen vacancies, which increase the pyrochlore cell volume (Eq. (3)):

$$MgO + 2Sm_{Sm}^{\times} + 2Zr_{Zr}^{\times} + 6O_O^{\times} \rightarrow Mg_{Zr}^{''} + V_O^{\bullet\bullet} + Sm_2Zr_2O_7. \quad (3)$$

It should be emphasized that Mg enters the zirconium sublattice of the $Sm_2Zr_2O_7$ pyrochlore in small amounts up to x ≤ 0.1 and $Sm_2Zr_{2-x}Mg_xO_{7-\delta}$ ($x = 0.05$, 0.1) solid solutions do not contain impurity phases. As the Mg content increases at $x = 0.2$ the system becomes non-single phase and contains an impurity of Sm-doped ZrO_2 (ICDD PDF 37-31). For the $Gd_2Zr_{2-x}Mg_xO_{7-\delta}$ system, the range of solid solutions becomes even narrower: an impurity of Gd doped ZrO_2 (ICDD PDF 42–1164, 73–1441) was found in $Gd_2Zr_{2-x}Mg_xO_{7-\delta}$ ($x = 0.1$).

If Mg resides on the Sm site, there is a different relationship between the eight-coordinate ionic radii, $Mg^{2+}_{CN8} = 0.89$ Å and $Sm^{3+}_{CN8} = 1.079$ Å, i.e., the ionic radius of Mg is noticeably smaller than that of Sm [39], and even the formation of oxygen vacancies according to scheme (4):

$$4MgO + 4Sm_{Sm}^{\times} + 2Zr_{Zr}^{\times} + 3O_O^{\times} \rightarrow 4Mg_{Sm}^{'} + 2Sm_{Zr}^{'} + 3V_O^{\bullet\bullet} + Sm_2Zr_2O_7. \quad (4)$$

causes no increase in unit-cell parameter or volume, unlike in the case of Mg doping on the Zr site. For $Sm_{2-x}Mg_xZr_2O_{7-\delta}$ ($x = 0$, 0.1, 0.3) system, the formation of a single-phase pyrochlore was also observed only up to a content of $x \leq 0.1$.

3.2. Microstructure of the $Ln_2Zr_2O_7$ (Ln = Sm, Gd)-based solid solutions Mg-doped on the Ln and Zr sites

We studied the microstructure of the $Sm_2Zr_{2-x}Mg_xO_{7-\delta}$ ($x = 0$, 0.05, 0.1, 0.2) and $Sm_{1.9}Mg_{0.1}Zr_2O_{7-\delta}$ pyrochlores prepared at 1600 °C. The data are presented in Fig. 4a–e. The single-phase $Sm_2Zr_{2-x}Mg_xO_{7-\delta}$ ($x = 0$, 0.1) materials range in grain size from 0.5 to 3 μm and have insignificant open porosity (Fig. 4a,c). The single-phase $Sm_2Zr_{2-x}Mg_xO_{7-\delta}$ ($x = 0.05$) has grain size from 0.5 to 1.5 (Fig. 4b) and very high density

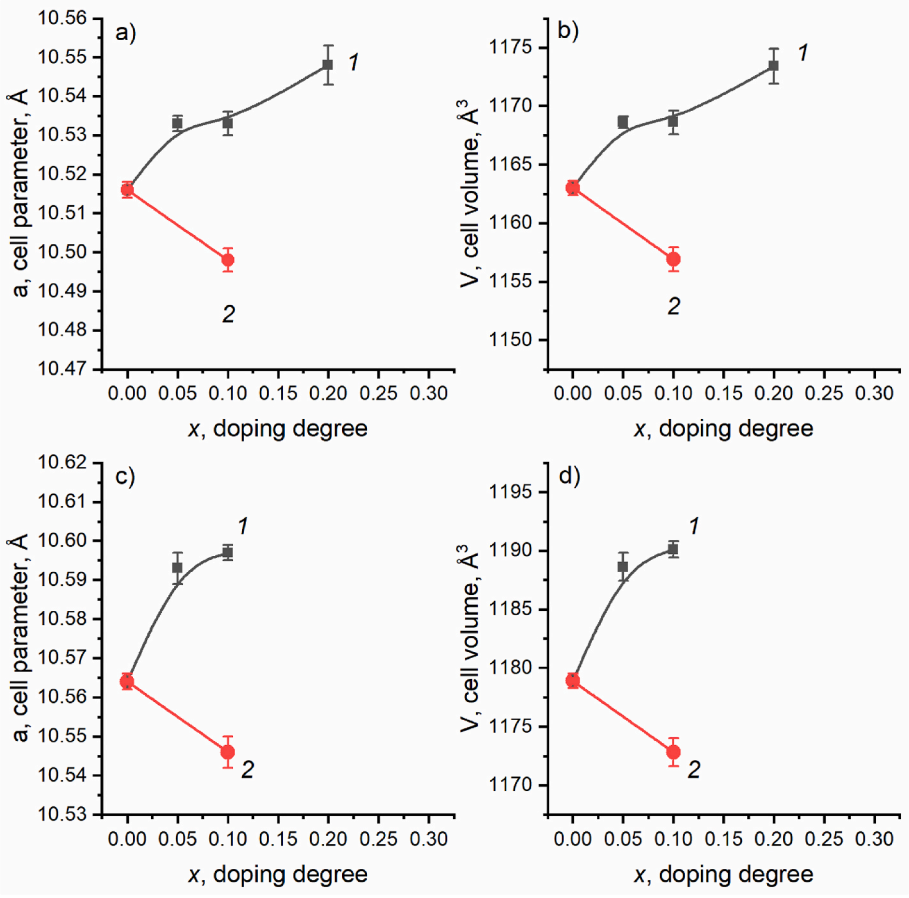

Fig. 3. Composition dependences of the unit-cell (a, c) parameter and (b, d) volume for the (a, b) gadolinium zirconates doped with Mg on the (1) Zr site $Gd_2Zr_{2-x}Mg_xO_{7-\delta}$ ($x = 0$, 0.05, 0.1, 0.2) and (2) Gd site $Gd_{2-x}Mg_xZr_2O_{7-\delta}$ ($x = 0$, 0.1) and (c, d) samarium zirconates doped with Mg on the (1) Zr site $Sm_2Zr_{2-x}Mg_xO_{7-\delta}$ ($x = 0$, 0.05, 0.1) and (2) Sm site $Sm_{2-x}Mg_xZr_2O_{7-\delta}$ ($x = 0$, 0.1).

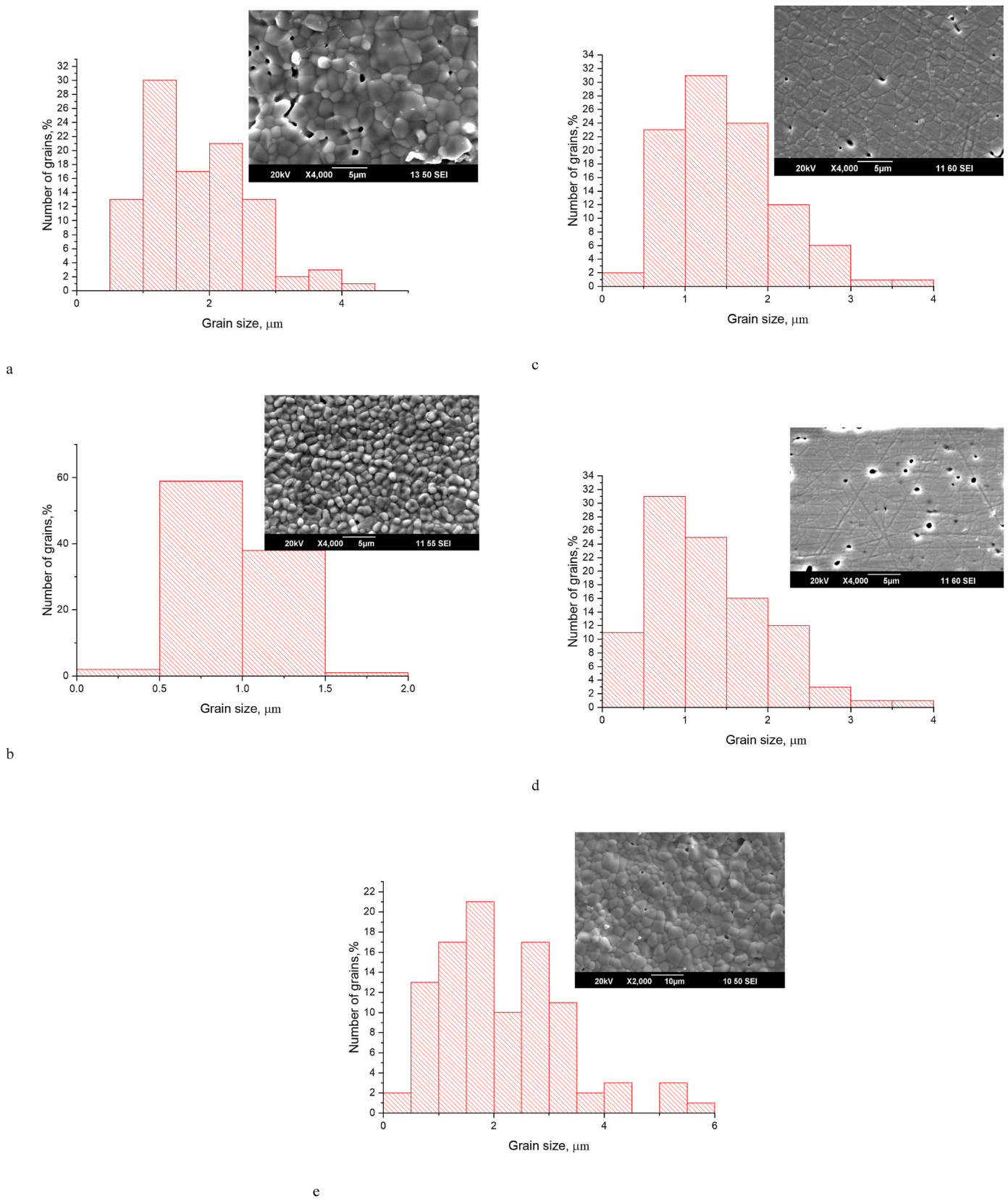

Fig. 4. Microstructure of the $Sm_2Zr_2O_7$-based solid solutions prepared by firing at 1600 °C for 4 h: (a) $Sm_2Zr_2O_7$ (b) $Sm_2Zr_{1.95}Mg_{0.05}O_{7-\delta}$; (c) $Sm_2Zr_{1.9}Mg_{0.1}O_{7-\delta}$; (d) $Sm_2Zr_{1.8}Mg_{0.2}O_{7-\delta}$; (e) $Sm_{1.9}Mg_{0.1}Zr_2O_{7-\delta}$.

~95.5 % (Table 1). The particle size distribution for the two-phase $Sm_2Zr_{2-x}Mg_xO_{7-\delta}$ ($x = 0.2$) material is slightly wider (from 0 to 3 μm) (Fig. 4d). The microstructure of $Sm_{1.9}Mg_{0.1}Zr_2O_{7-\delta}$ ranges widely in grain size: from 0 to 6 μm (Fig. 4e). On the whole, it is worth noting that doping with Mg improves the sintering behavior of the Sm-containing pyrochlore ceramics, which as a result have low open porosity (Table 1, sample 11).

The $Gd_2Zr_{2-x}Mg_xO_{7-\delta}$ ($x = 0.1$, 0.2) (Fig. 4b and c) and $Dy_2Zr_{2-x}Mg_xO_{7-\delta}$ ($x = 0.1$) (Fig. 5e) ceramics, containing Mg on the Zr site and prepared at 1600 °C as well, are more porous than $Gd_2Zr_2O_7$ and $Gd_{1.9}Mg_{0.1}Zr_2O_{7-\delta}$ (Fig. 5a,d). Note that the porosity of the ceramics increases with decreasing Ln ionic radius in the zirconates doped on the Zr site: $Ln_2Zr_{2-x}Mg_xO_{7-\delta}$ (Ln = Sm, Gd, Dy; $x = 0.1$) (Fig. 4c, Fig. 5b,e). Porosity makes ion transport more difficult. So the higher the porosity, the worse the ion transport.

The ceramics doped on the lanthanide site, $Ln_{1.9}Mg_{0.1}Zr_2O_{7-\delta}$ (Ln = Sm, Gd), showed much better sintering behavior (Fig. 4e and 5d). Clearly, the $Gd_{1.9}Mg_{0.1}Zr_2O_{7-\delta}$ ceramic (Fig. 5d) stands out among the Gd-containing samples studied here in that it consists of large grains (up to ~ 9 μm in size) and has a low pore density and highest relative density ~ 99 % (Table 1, sample 17).

3.3. Conductivity of the $Ln_2Zr_2O_7$ (Ln = Sm, Gd)-based solid solutions Mg-doped on the Ln and Zr sites

In this study, we used two synthesis temperatures, 1500 and 1600 °C, because too high a synthesis temperature can lead to both an increase in the density of the material, which is advantageous, and a uniform dopant distribution between the two cation sites, which is undesirable [36]. Fig. S2 and S3 show the typical view of the impedance spectra of $Sm_2Zr_{2-x}Mg_xO_{7-\delta}$ ($x = 0.05$) at 530 and 615 °C in dry and wet air, respectively, and an equivalent circuit used to fit these impedance spectra. Fig. S4 shows Arrhenius plots of conductivity for the $Ln_2Zr_{2-x}Mg_xO_{7-\delta}$ (Ln = Sm, Gd; $x = 0.05$, 0.1) ceramics prepared at 1500 °C. Fig. 6a shows Arrhenius plots of the total conductivity in dry and wet air of the $Sm_2Zr_2O_7$-based ceramics synthesized at 1600 °C: $Sm_2Zr_{2-x}Mg_xO_{7-\delta}$ ($x = 0$, 0.05, 0.1, 0.2) and $Sm_{2-x}Mg_xZr_2O_{7-\delta}$ ($x = 0.1$, 0.3). Fig. 6b shows Arrhenius plots of the total conductivity of $Sm_2Zr_{1.95}Mg_{0.05}O_{7-\delta}$ in different atmospheres (4-probe DC method). Fig. 7 demonstrates Arrhenius plots of the total conductivity in dry and wet air of the $Gd_2Zr_2O_7$-based ceramics synthesized at 1600 °C: $Gd_2Zr_{2-x}Mg_xO_{7-\delta}$ ($x = 0$, 0.05, 0.1, 0.2) and $Gd_{1.9}Mg_{0.1}Zr_2O_{7-\delta}$. Arrhenius plot of the total conductivity of $Dy_2Zr_{2-x}Mg_xO_{7-\delta}$ ($x = 0.1$) is also show in Fig. 7.

Firstly, it should be noted that the Sm and Gd-containing ceramics $Ln_2Zr_{2-x}Mg_xO_{7-\delta}$ (Ln = Sm, Gd; $x = 0.05$, 0.1) prepared at 1600 °C (Fig. 6a and 7) had higher conductivity than those synthesized at 1500 °C (Fig. S4). The activation energy for these ceramics is presented in Table 2. Note that the Sm-containing samples have a proton contribution in the range 300–600 °C and that the Gd-containing ceramics have lower total conductivity in this temperature range and higher oxygen ion conductivity above 800 °C in comparison with the Sm-containing ceramics doped on the same site.

Fig. 6a presents data for the Sm-containing ceramics prepared by firing at 1600 °C for 4 h, including undoped $Sm_2Zr_2O_7$. The conductivity of the $Sm_{1.9}Mg_{0.1}Zr_2O_{7-\delta}$ solid solution, doped with Mg on the Sm site, is seen to exceed that of $Sm_2Zr_2O_7$ doped on the Zr site ($Sm_2Zr_{2-x}Mg_xO_{7-\delta}$ ($x = 0.05$, 0.1, 0.2)) over the entire temperature range studied. Note also that the $Sm_2Zr_{2-x}Mg_xO_{7-\delta}$ ceramics have proton conductivity in the range 300–550 °C at degrees of substitution $x = 0.05$ and 0.1 and in the range 300–400 °C at $x = 0.2$. In this case, proton conduction is not intrinsic, but results from interaction of oxygen vacancies with water vapor from the ambient atmosphere:

$$H_2O + V_O^{\bullet\bullet} + O_O^{\times} \rightarrow 2(OH)_O^{\bullet} \quad (5)$$

In addition a complex oxide, undergoes classic quasi-chemical reactions with atmospheric oxygen (6):

$$\frac{1}{2}O_2 + V_O^{\bullet\bullet} \rightarrow O_O^{\times} + 2h^{\bullet} \quad (6)$$

According to (6), hole conduction is possible at elevated oxygen partial pressures. As a result, there will be a competition between atmospheric oxygen and water vapor for filling oxygen vacancies.

The 4-probe DC measurements were additionally carried out in dry and wet atmospheres (air and nitrogen) in order to confirm the presence of proton conductivity in $Sm_{1.95}Mg_{0.05}Zr_2O_{7-\delta}$. The proton conduction contribution was ascertained by comparing the conductivities measured in dry air ($pH_2O = 1{\cdot}10^{-4}$ atm., $pO_2 = 0.21$ atm.), wet air (pH_2O = 0.023–0.03 atm., pO_2 = 0.205–0.024 atm.), and wet nitrogen (pH_2O = 0.03 atm., $pO_2 = \sim 7{\cdot}10^{-5}$ atm.). For example, oxygen ion conductivity prevailed in dry air between 500 and 600 °C (Fig. 6b), with no proton contribution because pH_2O was very low, whereas in wet nitrogen and wet air (higher pH_2O and lower pO_2 in comparison with dry air) there was proton conduction along with oxygen ion conduction. Thus, the difference between the conductivities in wet nitrogen and dry air was due to proton conduction in wet nitrogen. The obtained results (Fig. 6b) correlate with the impedance (2-probe AC method) data in wet air. The estimated values of proton conductivity in wet air are close and equal to 9×10^{-5} S/cm (4-probe DC method) and 1×10^{-4} S/cm (2-probe AC method) at 500 °C.

Among the samarium zirconates studied here, high proton conductivity (1×10^{-4} S/cm at 500°C) is offered by the $Sm_{1.95}Mg_{0.05}Zr_2O_{7-\delta}$ solid solution. At the same time, no proton conduction was detected in $Sm_{1.9}Mg_{0.1}Zr_2O_{7-\delta}$. Thus, like in the case of yttrium doping of various $Ln_2Zr_2O_7$ zirconates on the Zr site ($Ln_2Zr_{1.8}Y_{0.2}O_{7-\delta}$ (Ln = La, Nd, Sm, Gd, and Er)) (measurements in H_2) [33], Zr-site doping of $Sm_2Zr_2O_7$ with Mg to $x = 0.05$, 0.1, and 0.2 gives rise to a proton contribution in wet air, but an increase in Mg content leads to a decrease in both total and proton conductivity. Thus, Zr-site doping leads to proton conduction in wet air even in the case of Mg, a poorly hydratable cation [34]. It should be noted that at temperatures below 450 °C, pure $Sm_2Zr_2O_7$ also exhibits higher conductivity in wet air than in dry air (Fig. 5a, curve 6). According to Shinozaki et al. [41], $Sm_2Zr_2O_7$, like $Gd_2Zr_2O_7$ [25], has a hole conductivity contribution at high oxygen partial pressures. The high conductivity of $Sm_2Zr_2O_7$ with a density of 87.4 % in dry air is of mixed type (oxygen ions and holes). In this case, the conductivity is also sensitive to the humidification of the system [42].

In comparing results of Sm-site doping with Mg and Ca, it should be noted that $Sm_{1.9}Ca_{0.1}Zr_2O_{7-\delta}$ has proton conductivity [22], whereas $Sm_{1.9}Mg_{0.1}Zr_2O_{7-\delta}$ does not, in accordance with the low hydratability of Mg cations [34]. The oxygen ion conductivity of the zirconates (T> 800°C) is independent of the dopant (Ca^{2+} [22] or Mg^{2+} [this work]).

Table 3 lists the activation energies for conduction in the Mg consisting zirconates ($T_{syn.}$ = 1600 °C) in dry and wet air between 300 and 600 °C. The activation energy in the $Sm_2Zr_{2-x}Mg_xO_{7-\delta}$ ($x = 0.05$, 0.1, 0.2) series in dry air is 0.95, 0.93, and 0.9 eV, respectively, and that in wet air is 0.85, 0.86, and 0.88 eV (Table 3). With increasing Mg content, the activation energy in wet air rises and that in dry air decreases. The activation energy for conduction in $Sm_2Zr_{2-x}Mg_xO_{7-\delta}$ ($x = 0.05$, 0.1) in wet air is lower than that in dry air. In dry air, the majority charge carriers are oxygen ions and holes, whereas those in wet air are oxygen ions, holes, and protons. Protons have a small mass and small size, so their mobility is higher than that of oxygen ions. As a result, the energy needed to overcome the potential barrier to proton transport is lower [43]. The higher the mobility, the higher the conductivity (all else being equal). An increase in conductivity usually leads to a decrease in activation energy [44,45].

Fig. 7 presents data for the Gd-containing ceramics prepared by firing at 1600 °C for 4 h. The conductivity of the $Gd_2Zr_2O_7$ doped with Mg on the Gd site ($Gd_{1.9}Mg_{0.1}Zr_2O_{7-\delta}$) (Fig. 7, curve 4) is seen to exceed

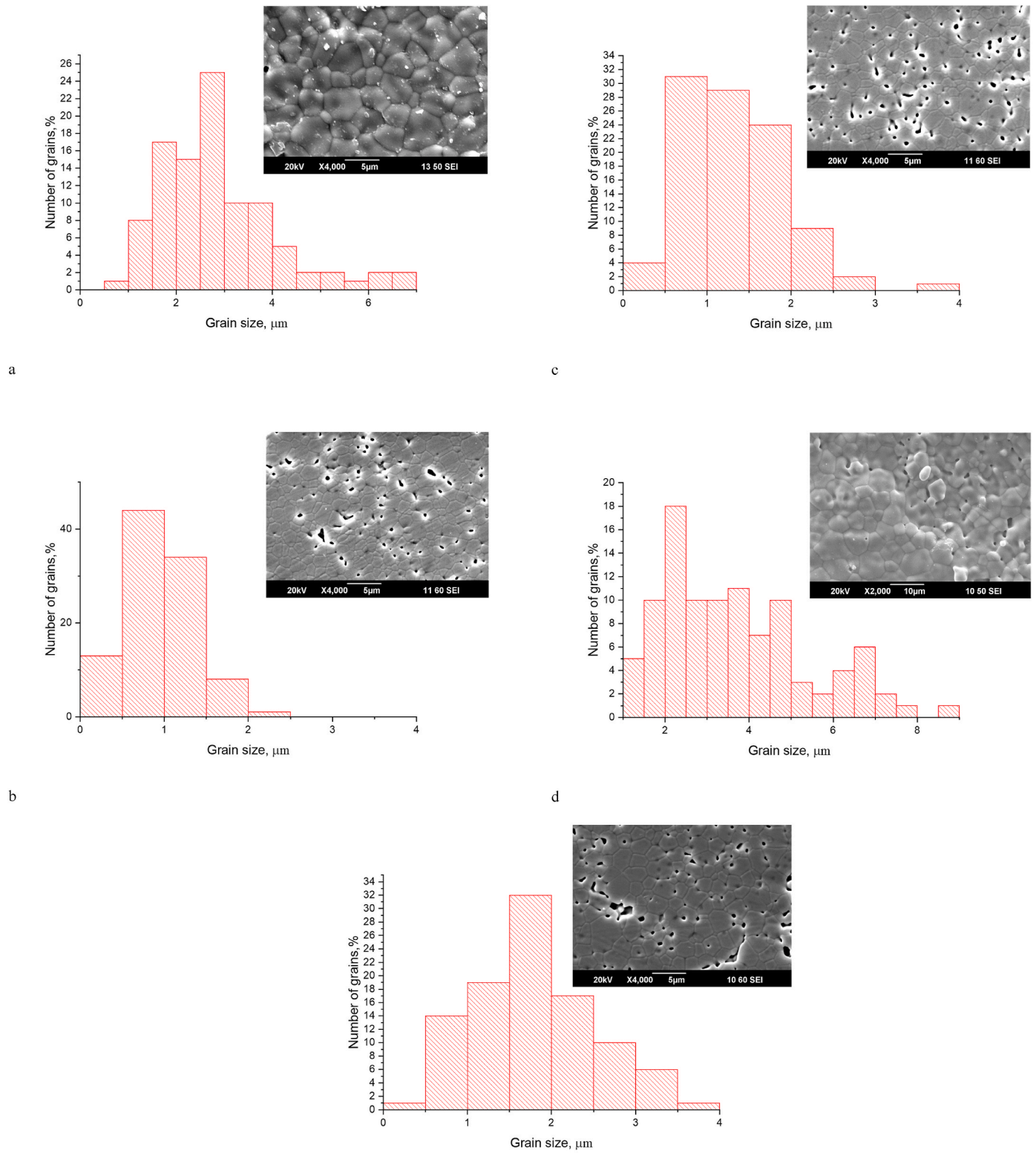

Fig. 5. Microstructure of the $Gd_2Zr_2O_7$-based and $Dy_2Zr_{1.9}Mg_{0.1}O_x$ solid solutions prepared by firing at 1600 °C for 4 h:
a $Gd_2Zr_2O_7$;
b $Gd_2Zr_{1.9}Mg_{0.1}O_{7-\delta}$;
c $Gd_2Zr_{1.8}Mg_{0.2}O_{7-\delta}$;
d $Gd_{1.9}Mg_{0.1}Zr_2O_{7-\delta}$;
e $Dy_2Zr_{1.9}Mg_{0.1}O_{7-\delta}$.

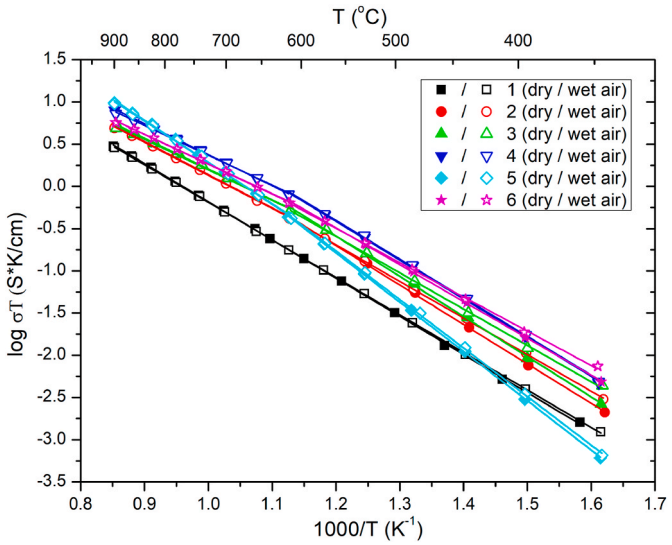

Fig. 6a. Arrhenius plots of the total conductivity in dry and wet air of the $Sm_2Zr_2O_7$-based ceramics synthesized at 1600 °C:
(1) $Sm_2Zr_{1.8}Mg_{0.2}O_{7-\delta}$;
(2) $Sm_2Zr_{1.9}Mg_{0.1}O_{7-\delta}$;
(3) $Sm_2Zr_{1.95}Mg_{0.05}O_{7-\delta}$;
(4) $Sm_{1.9}Mg_{0.1}Zr_2O_{7-\delta}$;
(5) $Sm_{1.7}Mg_{0.3}Zr_2O_{7-\delta}$;
(6) $Sm_2Zr_2O_7$.

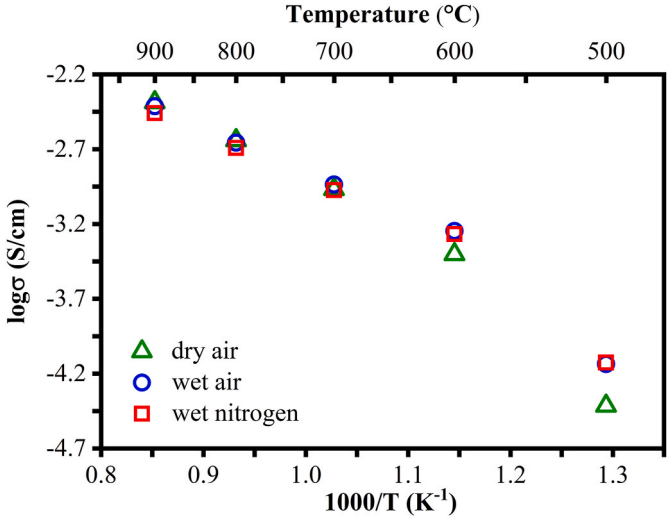

Fig. 6b. Arrhenius plots of the total conductivity of $Sm_2Zr_{1.95}Mg_{0.05}O_{7-\delta}$ in different atmospheres (4-probe DC method).

that of the Zr-site-doped $Gd_2Zr_2O_7$ ($Gd_2Zr_{2-x}Mg_xO_{7-\delta}$ (x = 0.05, 0.1, 0.2)) (Fig. 7, curves 1–3) over the entire temperature range studied. The fluorite-like $Dy_2Zr_{1.9}Mg_{0.1}O_{7-\delta}$ ceramics have the lowest oxygen ion conductivity (Fig. 7, curve 5). Curve 6 in Fig. 7 presents data for undoped $Gd_2Zr_2O_7$ studied previously in air. The oxygen ion conductivity of $Gd_{1.9}Mg_{0.1}Zr_2O_{7-\delta}$ is seen to exceed that of $Gd_2Zr_2O_7$, whereas Zr-site doping in $Gd_2Zr_{2-x}Mg_xO_{7-\delta}$ (x = 0.05, 0.1, 0.2) reduces its conductivity, which decreases with increasing Mg content on the Zr site.

However, no proton conductivity was detected in this case by direct measurements on the Gd-containing samples in our cell. That there is no appreciable proton contribution in the range 300–600 °C is also evidenced by the activation energy for conduction obtained in dry and wet air (Table 4). E_a is seen to be insensitive to wet air. In comparing the oxygen ion conductivity of the Gd-containing solid solutions doped with

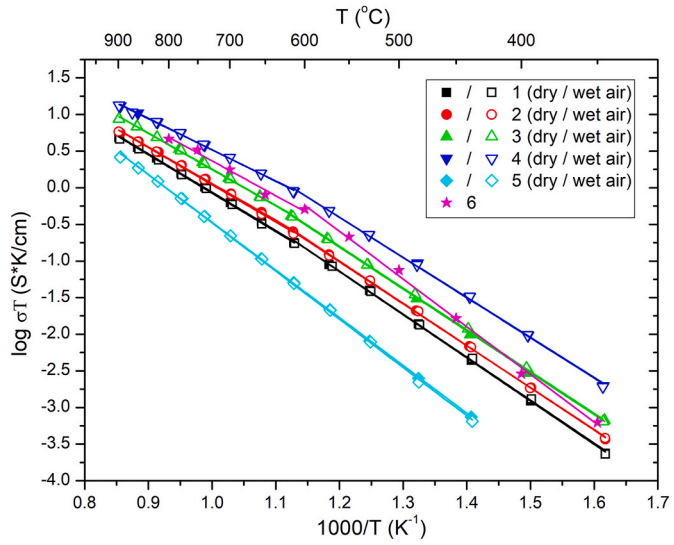

Fig. 7. Arrhenius plots of the total conductivity in dry and wet air of Arrhenius plots of the total conductivity in dry and wet air of the $Gd_2Zr_2O_7$ -based and $Dy_2Zr_{1.9}Mg_{0.1}O_{7-\delta}$ ceramics synthesized at 1600 °C
(1) $Gd_2Zr_{1.8}Mg_{0.2}O_{7-\delta}$;
(2) $Gd_2Zr_{1.9}Mg_{0.1}O_{7-\delta}$;
(3) $Gd_2Zr_{1.95}Mg_{0.05}O_{7-\delta}$;
(4) $Gd_{1.9}Mg_{0.1}Zr_2O_{7-\delta}$;
(5) $Dy_2Zr_{1.9}Mg_{0.1}O_{7-\delta}$;
(6) $Gd_2Zr_2O_7$.

Table 2
Activation energy for the total conductivity of the solid solutions prepared at 1500 °C, as determined by measurements between 300 and 900 °C in dry and wet air.

Composition	Atmosphere	E_a, eV
$Sm_2Zr_{1.9}Mg_{0.1}O_{7-\delta}$	Dry air	0.93
	Wet air	0.90
$Sm_2Zr_{1.95}Mg_{0.05}O_{7-\delta}$	Dry air	0.86
	Wet air	0.82
$Gd_2Zr_{1.9}Mg_{0.1}O_{7-\delta}$	Dry air	1.11
	Wet air	1.10
$Gd_2Zr_{1.95}Mg_{0.05}O_{7-\delta}$	Dry air	1.08
	Wet air	1.08

Table 3
Activation energy of the $Sm_2Zr_2O_7$-based solid solutions prepared at 1600 °C, as determined by measurements between 300 and 900 °C in dry and wet air.

Sample	Composition	Temperature range, °C	Activation energy, eV	
			Dry air	Wet air
3	$Sm_2Zr_{1.8}Mg_{0.2}O_{7-\delta}$	300–900	0.90	0.88
2	$Sm_2Zr_{1.9}Mg_{0.1}O_{7-\delta}$	300–600	0.93	0.86
		600–900	0.78	0.78
1	$Sm_2Zr_{1.95}Mg_{0.05}O_{7-\delta}$	300–600	0.95	0.85
		600–900	0.73	0.72
11	$Sm_{1.9}Mg_{0.1}Zr_2O_{7-\delta}$	300–600	0.91	0.91
		600–900	0.73	0.70
12	$Sm_{1.7}Mg_{0.3}Zr_2O_{7-\delta}$	300–600	1.16	1.14
		600–900	0.99	0.97
7	$Sm_2Zr_2O_7$	300–600	0.87	0.81
		600–900	0.70	0.70

Ca and Mg, it is worth noting that the conductivity of $Gd_{1.9}Mg_{0.1}Zr_2O_{7-\delta}$ (5×10^{-3} S/cm at 700 °C) is four times that of $Gd_{1.9}Ca_{0.1}Zr_2O_{7-\delta}$ [22].

Specific features of oxygen transport in $Gd_{1.9}Mg_{0.1}Zr_2O_{7-\delta}$ were studied using oxygen isotope exchange with $^{18}CO_2$ in a flow reactor in temperature-programmed mode or under isothermal conditions [46].

Table 4
Activation energy of the $Gd_2Zr_2O_7$-based solid solutions prepared at 1600 °C, as determined by measurements between 300 and 900 °C in dry and wet air.

Sample	Composition	Temperature range, °C	Activation energy, eV	
			Dry air	Wet air
16	$Gd_2Zr_{1.8}Mg_{0.2}O_{7-\delta}$	300–600	1.17	1.17
		600–900	1.04	1.04
15	$Gd_2Zr_{1.9}Mg_{0.1}O_{7-\delta}$	300–600	1.15	1.14
		600–900	0.99	1.01
14	$Gd_2Zr_{1.95}Mg_{0.05}O_{7-\delta}$	300–600	1.13	1.13
		600–900	0.98	0.98
17	$Gd_{1.9}Mg_{0.1}Zr_2O_{7-\delta}$	300–600	1.09	1.09
		600–900	0.85	0.84
18	$Dy_2Zr_{1.9}Mg_{0.1}O_{7-\delta}$	400–900	1.29	1.31
13	$Gd_2Zr_2O_7$	300–600	1.29	–
		600–800	0.94	–

According to mathematical modelling results, there was very fast grain-boundary diffusion ($D \sim 10^{-9} - 10^{-8}$ cm^2/s at 700 °C) involving 5 % of the total amount of oxygen. Presumably, there are three diffusion channels in the grain bulk, related to oxygen transport along the following bond chains in the pyrochlore structure: Zr-O-Zr, Zr-O-Gd, and Gd-O-Gd. The modelling results are in excellent agreement with experimental data [46].

Comparison with conductivity of $Nd_2Zr_{2-x}Mg_xO_{7-x}$ (x = 0.01) neodymium zirconate-based ceramics in N_2 atmosphere [38] shows that the 800 °C oxygen ion conductivity of $Ln_2Zr_{2-x}Mg_xO_{7-\delta}$ (Ln = Sm, Gd; x = 0.05, 0.1) is one order of magnitude higher. Unfortunately, the conductivity of $Nd_2Zr_{2-x}Mg_xO_{7-x}$ (x = 0.01) depends strongly on the atmosphere, leading to *p*-type semiconductivity under pure O_2 atmosphere [38]. Thus, like in the case of the undoped $Ln_2Zr_2O_7$ (Ln = Nd, Sm, Gd) zirconates [11], above 700 °C the oxygen ion conductivity of the $Ln_2Zr_{2-x}Mg_xO_{7-\delta}$ (Ln = Nd, Sm, Gd) solid solutions, doped with Mg on the Zr site, increases with decreasing Ln ionic radius.

3.4. Thermogravimetric analysis of $Sm_2Zr_{2-x}Mg_xO_{7-\delta}$ (x = 0.05) in dry oxygen

Fig. 8 presents TG data obtained during heating in dry oxygen for $Sm_2Zr_{2-x}Mg_xO_{7-\delta}$ (x = 0.05) with a hydrostatic density above 95 % (Table 1), which has a proton contribution to conductivity. Three weight loss steps can be distinguished in the first heating cycle. The first step, between 50 and 420 °C, is the removal of surface water, water in the pores of the material, and hydroxyl ions. The second step, up to 660 °C, corresponds to the removal of hydroxyl ions and some of the structurally bound protons [47]. The process above 660 °C and up to 1000 °C is gradual removal of structurally bound water and interstitial protons [47]. The weight loss curve is seen to not plateau even after the second heating. We believe that this is due to the hygroscopicity of the ceramic. During the first heating, there possibly were carbon impurities, which burned in oxygen. The final amount of such impurities in terms of carbon (graphite) did not exceed 0.2–0.5 wt % [48]. It seems likely that the $Sm_2Zr_{2-x}Mg_xO_{7-\delta}$ (x = 0.05) powder had a tendency to pick up water and CO_2 during cooling, as evidenced by the fact that the weight loss curve did not plateau even after the second heating.

The stability of the single-phase $Sm_2Zr_{2-x}Mg_xO_{7-\delta}$ (x = 0.05) material under reducing conditions was studied using the TPR method and these data are presented in Fig. S5. These results show that the $Sm_2Zr_{2-x}Mg_xO_{7-\delta}$ (x = 0.05) ceramic was not reduced. H_2 absorption was at the level of detector sensitivity.

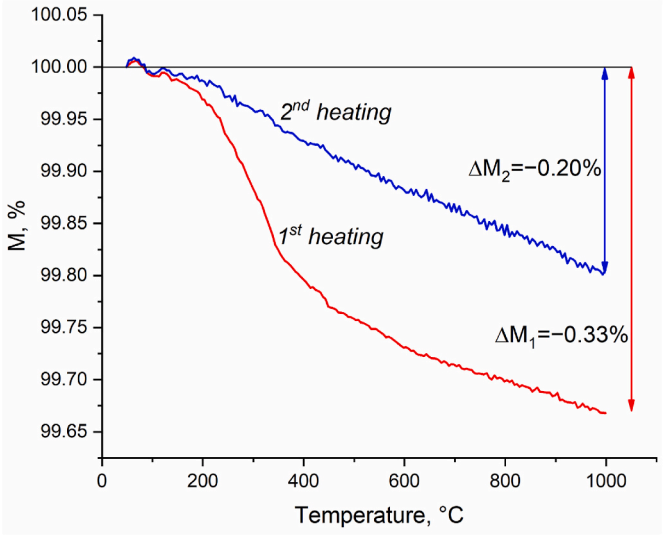

Fig. 8. Weight loss (TG) data obtained for the $Sm_2Zr_{1.95}Mg_{0.05}O_{7-\delta}$ powder during two sequential heating cycles in oxygen.

3.5. Dependence of the total conductivity on oxygen partial pressure for $Ln_{1.9}Mg_{0.1}Zr_2O_{7-\delta}$ (Ln = Sm, Gd; x = 0.1) in the high temperature range ($700 \leq T \leq 1000$ °C)

The width of the oxygen pressure range where ion conduction prevailed was assessed for the materials doped with Mg on the lanthanide site and having the highest oxygen on conductivity: $Ln_{1.9}Mg_{0.1}Zr_2O_{7-\delta}$ (Ln = Sm, Gd; x = 0.1).

Fig. 9 presents log-log plots of total conductivity versus oxygen partial pressure at high temperatures (700–1000 °C), demonstrating that conductivity remains independent of oxygen partial pressure, a hallmark of pure ionic conductors. It is worth noting that at these high

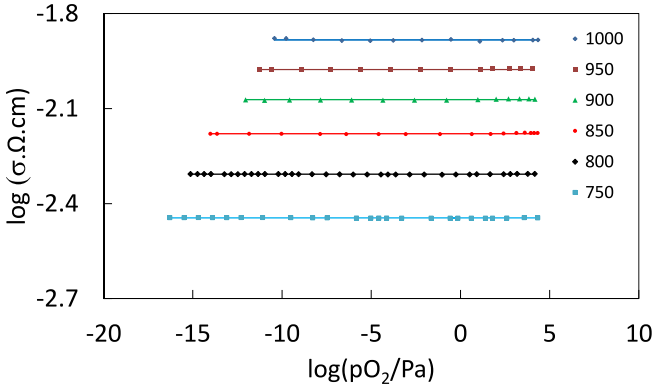

(a)

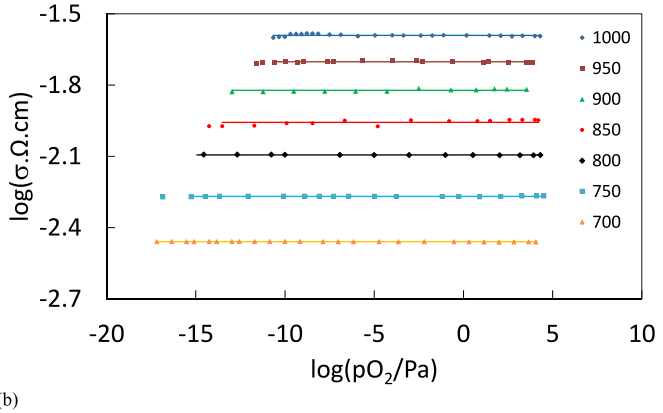

(b)

Fig. 9. Log–log plots of total conductivity vs. oxygen partial pressure for (a) $Sm_{1.9}Mg_{0.1}Zr_2O_{7-\delta}$ and (b) $Gd_{1.9}Mg_{0.1}Zr_2O_{7-\delta}$ in the range 700–1000 °C.

temperatures, proton conductivity is typically negligible, leaving the oxygen ion contribution as the single component of the total conductivity. Thus, the oxygen partial pressure having no effect on conductivity indicates that we are in a so-called electrolytic conduction range, where the oxygen ion contribution to conductivity prevails and there is no *n*- or *p*-type electronic conductivity. It is also worth noting that the oxygen stoichiometry of mixed oxides is determined by dopant concentration. Moreover, the fact that the conductivity is independent of pO_2 indicates that the material has stable composition and that, under the conditions of our measurements, its oxygen stoichiometry remains unchanged, being insensitive to pO_2. Otherwise, the conductivity would be observed to vary with pO_2. The absence of hole conduction at high oxygen partial pressures is an obvious advantage of the pyrochlores over many perovskites. It is such materials, having high oxygen ion conductivity and no hole contribution in air, which are needed for practical application in SOFCs [29].

The conductivity of the $Gd_{1.9}Mg_{0.1}Zr_2O_{7-\delta}$ solid solution (Fig. 9a) is seen to exceed that of $Sm_{1.9}Mg_{0.1}Zr_2O_{7-\delta}$ (Fig. 9b), reaching 5.5×10^{-3} S/cm at 700 °C, which approaches the level of practical importance at this temperature: 8.4×10^{-3} S/cm [1]. The activation energy for oxygen ion conduction above 700 °C is 0.68 eV for the samarium zirconate $Sm_{1.9}Mg_{0.1}Zr_2O_{7-\delta}$ and 0.8 eV for the gadolinium zirconate $Gd_{1.9}Mg_{0.1}Zr_2O_{7-\delta}$. These values approach those obtained in dry air by impedance spectroscopy: 0.73 and 0.85 eV, respectively (Tables 3 and 4).

3.6. Analysis of potential relationship between microstructure and conductivity in ionic conductors under investigation

The average grain size of the ceramics doped with Mg at the *Ln* site, $Ln_{2-x}Mg_xZr_2O_{7-\delta}$ (*Ln* = Sm, Gd; $x = 0.1$), is larger than that of the ceramics doped with Mg at the zirconium site and is 1.86 μm for $Sm_{1.9}Mg_{0.1}Zr_2O_{7-\delta}$ and 3.42 μm for $Gd_{1.9}Mg_{0.1}Zr_2O_{7-\delta}$, respectively (Table 1). The samarium sample is more homogeneous than the gadolinium sample (Fig. 4e and 5d). The particle size distribution is similar for pure $Sm_2Zr_2O_7$ and doped $Sm_{1.9}Mg_{0.1}Zr_2O_{7-\delta}$ (Fig. 4a and d). The main fraction is between 0.5 and 3.5 μm. In the gadolinium system, the similarity of the grain size distributions for $Gd_2Zr_2O_7$ and doped $Gd_{1.9}Mg_{0.1}Zr_2O_{7-\delta}$ can also be observed (Fig. 5a and d) However, in the gadolinium system there are two fractions of grains: smaller and larger. In $Gd_2Zr_2O_7$, the smaller fraction is from 0 to 5.5 μm and the larger fraction is from 5.5 to 8.0 μm. In $Gd_{1.9}Mg_{0.1}Zr_2O_{7-\delta}$, the smaller fraction is 0.5–4.5 μm and the larger is 4.5–7.0 μm. However, the oxygen-ion conductivity is high in both ceramics doped with magnesium in the Ln sublattice, mainly due to the appearance of oxygen vacancies in pyrochlore, which increase the oxygen transport of the electrolyte, and the high density of Mg-containing samples.

Among the proton conducting ceramics $Sm_2(Zr_{2-x}Mg_x)O_{7-\delta}$ ($x = 0.05$, 0.1, 0.2), the maximum proton conductivity was found for $Sm_2(Zr_{2-x}Mg_x)O_{7-\delta}$ ($x = 0.05$) with the narrowest grain distribution from 0.5 to 1.5 μm and with the highest density among the studied samarium samples (Fig. 4b, Table 1). The appearance of an impurity phase (according to the XRD data) in the form of dark inclusions for the two-phase material $Sm_2(Zr_{2-x}Mg_x)O_{7-\delta}$ ($x = 0.2$) (Fig. 4d) leads to a decrease of the total conductivity by 6–7 times. It is interesting to note that in the Gd system the total conductivity of the two-phase material $Gd_2(Zr_{2-x}Mg_x)O_{7-\delta}$ ($x = 0.1$) according to X-ray diffraction, decreases insignificantly.

Analysis of the Arrhenius dependencies of the GdZrMgO system shown in Fig. 6 indicates that for oxygen-ion conductors, the structural rearrangement from pyrochlore to fluorite is more critical factor than the presence of the impurity fluorite phase, Gd-doped ZrO_2 in pyrochlore. The total conductivity of the two-phase material $Gd_2(Zr_{2-x}Mg_x)O_{7-\delta}$ ($x = 0.1$) is higher than that of the single-phase fluorite-like $Gd_2(Zr_{2-x}Mg_x)O_{7-\delta}$ ($x = 0.2$) and $Dy_2(Zr_{2-x}Mg_x)O_{7-\delta}$ ($x = 0.1$) materials (Fig. 7).

4. Conclusions

The electrical conductivity of zirconate pyrochlores with the general compositions $Ln_2Zr_{2-x}Mg_xO_{7-\delta}$ (*Ln* = Sm, Gd; $x = 0$, 0.05, 0.1, 0.2), $Ln_{2-x}Mg_xZr_2O_{7-\delta}$ (*Ln* = Sm, Gd; $x = 0$, 0.1, 0.3), and $Dy_2(Zr_{2-x}Mg_x)O_{7-\delta}$ ($x = 0.1$) has been measured as a function of temperature between 300 and 900 °C in dry and wet air. In wet air, the $Sm_2Zr_{2-x}Mg_xO_{7-\delta}$ ($x = 0.05$, 0.1, 0.2) materials have proton conductivity, which is maximal, 1×10^{-4} S/cm at 500 °C, in $Sm_2Zr_{2-x}Mg_xO_{7-\delta}$ ($x = 0.05$), the densest ceramic (95.5 % density), and decreases with increasing Mg content. The same proton conductivity was previously found in $Sm_{2-x}Ca_xZr_2O_{7-\delta}$ ($x = 0.05$; 0.1) Ca-containing zirconates [22]. Note that $La_2(Zr_{1.985}Ca_{0.015})O_{7-\delta}$ was reported to have such proton conductivity in wet hydrogen [19]. Total conductivity vs. oxygen partial pressure data for the $Sm_{2-x}Mg_xZr_2O_{7-\delta}$ ($x = 0.1$) zirconates demonstrate that they have no *p*-type conductivity at high oxygen partial pressures up to 10^4 Pa, which is their advantage over Ca-doped zirconates with the same stoichiometries [22] and pure $Sm_2Zr_2O_7$ [41].

Among the Sm-containing ceramics, the highest oxygen ion conductivity, 5×10^{-3} S/cm at 750 °C, is offered by $Sm_{1.9}Mg_{0.1}Zr_2O_{7-\delta}$.

In the $Gd_2Zr_{2-x}Mg_xO_{7-\delta}$ ($x = 0.05$, 0.1, 0.2) series, no proton conduction has been detected under the conditions of this study, but the total conductivity of these materials decreases with increasing Mg content, like in the case of the Sm-containing materials having the same doping levels on the Zr site. The oxygen ion conductivity of $Gd_2Zr_{2-x}Mg_xO_{7-\delta}$ ($x = 0.05$, 0.1, 0.2) is lower than that of $Gd_{1.9}Mg_{0.1}Zr_2O_{7-\delta}$ (5.5×10^{-3} S/cm at 700 °C). Mg doping on the Zr site reduces the total conductivity of the zirconate solid solutions, whereas Mg doping on the Gd site increases it compared to undoped $Gd_2Zr_2O_7$.

The highest oxygen ion conductivity among the Mg-doped zirconates has been offered by $Gd_{1.9}Mg_{0.1}Zr_2O_{7-\delta}$ (5.5×10^{-3} S/cm at 700°C), and this value approaches the level needed for utilizing the material as a solid electrolyte (8.4×10^{-3} S/cm at 700 °C). An important point is that it contains neither lanthanum nor alkaline-earth metals, which will undoubtedly be favorable for long-term operation of this material as a SOFC solid electrolyte.

To summarize, all else being equal (e.g. the same B cation), proton conduction in $A_2B_2O_7$ pyrochlores can be determined by the nature of the A cations, namely, the rare-earth cations in the compounds under consideration. The ionic radius of the rare-earth cations determines the free volume in their unit cells, the feasibility of spatial reorientation of protons relative to oxygens, and hence the feasibility of proton transport.

CRediT authorship contribution statement

N.V. Lyskov: Visualization, Resources, Methodology, Investigation. **I.V. Kolbanev:** Investigation. **A.B. Borunova:** Investigation. **G.A. Vorobieva:** Visualization, Investigation, Formal analysis. **J.C.C. Abrantes:** Software, Methodology, Investigation, Formal analysis. **E. Gomes:** Investigation, Formal analysis. **N.A. Danilov:** Visualization, Investigation, Formal analysis. **D.A. Medvedev:** Data curation. **A.V. Shlyakhtina:** Writing – review & editing, Writing – original draft, Project administration, Methodology, Investigation, Data curation, Conceptualization.

Declaration of competing interest

The authors declare that they have no known competing financial interests or personal relationships that could have appeared to influence the work reported in this paper.

Acknowledgments

This study was carried out as part of the state assignment on the topic

"Interdisciplinary approaches to the creation and study of micro-/nanostructured systems" (registration no. 125012200595-8). Conductivity measurements of the samples were performed in accordance with the state task for FRC PCP and MC RAS (the state registration number 124013000692-4). The authors thank D.N. Stolbov for his studies of the microstructure of ceramics.

Appendix A. Supplementary data

Supplementary data to this article can be found online at https://doi.org/10.1016/j.ceramint.2025.05.015.

References

[1] J. Zhang, C. Lenser, N.H. Menzler, O. Guillon, Comparison of solid oxide fuel cell (SOFC) electrolyte materials for operation at 500 °C, Solid State Ionics 344 (2020) 115138, https://doi.org/10.1016/j.ssi.2019.115138.

[2] T.-H. Yeh, W.-C. Hsu, C.-C. Chou, Mechanical and electrical properties of ZrO2 (3Y) doped with $RENbO_4$ (RE = Yb, Er, Y, Dy, Y, Nd, Sm, nd), J. Phys. IV 128 (2005) 213–219, https://doi.org/10.1051/jp4:2005128032.

[3] S. Yoon, T. Noh, W. Kim, J. Choi, H. Lee, Structural parameters and oxygen-ion conductivity of Y_2O_3–ZrO_2 and MgO–ZrO_2 at high temperature, Ceram. Int. 39 (2013) 9247–9251, https://doi.org/10.1016/j.ceramint.2013.05.032.

[4] C. Xia, M. Liu, Microstructures, conductivities, and electrochemical properties of $Ce_{0.9}Gd_{0.1}O_2$ and GDC–Ni anodes for low-temperature SOFCs, Solid State Ionics 152–153 (2002) 423–430, https://doi.org/10.1016/S0167-2738(02)00381-8.

[5] B. Li, X. Wei, W. Pan, Improved electrical conductivity of $Ce_{0.9}Gd_{0.1}O_{1.95}$ and $Ce_{0.9}Sm_{0.1}O_{1.95}$ by co-doping, Int. J. Hydrogen Energy 35 (2020) 3018–3302, https://doi.org/10.1016/j.ijhydene.2009.07.002.

[6] Z. Gao, L.V. Mogni, E.C. Miller, J.G. Railsback, S.A. Barnett, A perspective on low-temperature solid oxide fuel cells, Energy Environ. Sci. 9 (2016) 1602–1644, https://doi.org/10.1039/C5EE03858H.

[7] D.-S. Lee, W.S. Kim, S.H. Choi, J. Kim, H.-W. Lee, J.-H. Lee, Characterization of ZrO2 co-doped with Sc_2O_3 and CeO_2 electrolyte for the application of intermediate temperature SOFCs, Solid State Ionics 176 (2005) 33–39, https://doi.org/10.1016/j.ssi.2004.07.013.

[8] A. Kumar, A. Jaiswal, M. Sanbui, S. Omar, Scandia stabilized zirconia-ceria solid electrolyte (xSc1CeSZ, 5 < x < 11) for IT-SOFCs: structure and conductivity studies, Scripta Mater. 121 (2016) 10–13, https://doi.org/10.1016/j.scriptamat.2016.04.023.

[9] M. Shimazu, K. Yamaji, H. Kishimoto, A. Ueno, T. Isobe, K.-i. Katsumata, H. Yokokawa, K. Okada, Stability of Sc_2O_3 and CeO_2 co-doped ZrO_2 electrolyte during the operation of solid oxide fuel cells: part III. Detailed mechanism of the decomposition, Solid State Ionics 224 (2012) 6–14, https://doi.org/10.1016/j.ssi.2012.06.025.

[10] M. Shimazu, T. Isobe, S. Ando, K. Hiwatashi, A. Ueno, K. Yamaji, H. Kishimoto, H. Yokokawa, A. Nakajima, K. Okada, Stability of Sc_2O_3 and CeO_2 co-doped ZrO_2 electrolyte during the operation of solid oxide fuel cells, Solid State Ionics 182 (2011) 120–126, https://doi.org/10.1016/j.ssi.2010.08.030.

[11] H. Yamamura, H. Nishino, K. Kakinuma, K. Nomura, Electrical conductivity anomaly around fluorite-pyrochlore phase boundary, Solid State Ionics 158 (2003) 359–365, https://doi.org/10.1016/S0167-2738(02)00874-3.

[12] H. Nishino, H. Yamamura, K. Arai, K. Kakinuma, K. Nomura, Effect of cation radius ratio and unit cell free volume on oxide-ion conductivity in oxide systems with pyrochlore-type composition, Ceram. Soc. Japan. 112 (2004) 541–546, https://doi.org/10.2109/jcersj.112.541.

[13] A.V. Shlyakhtina, K.S. Pigalskiy, Tolerance factor as the basic criterion in searching for promising oxygen-ion and proton conductors among $Ln_{2-x}D_xM_2O_{7-\delta}$ (Ln = La-Lu; M= Sn, Ti, Zr, Hf; D= Sr, Ca, Mg; x = 0, 0.1) 3+/4+ pyrochlores, Mater. Res. Bull. 116 (2019) 72–78, https://doi.org/10.1016/j.materresbull.2019.04.021.

[14] A.V. Shlyakhtina, L.G. Shcherbakova, New solid electrolytes of the pyrochlore family, Russ. J. Electrochem. 1 (2012) 1–25, https://doi.org/10.1134/S1023193512010144.

[15] J.A. Díaz-Guillén, M.R. Díaz-Guillén, J.M. Almanza, A.F. Fuentes, Santamaría, C. León, Effect of La substitution for Gd in the ionic conductivity and oxygen dynamics of fluorite-type $Gd_2Zr_2O_7$, J. Phys. Condens. Matter 19 (2007) 356212, https://doi.org/10.1088/0953-8984/19/35/356212.

[16] J.A. Díaz-Guillén, M.R. Díaz-Guillén, K.P. Padmasree, A.F. Fuentes, J. Santamaría, C. León, High ionic conductivity in the pyrochlore-type $Gd_{2-y}La_yZr_2O_7$ solid solution ($0 \le y \le 1$), Solid State Ionics 179 (2008) 2160–2164, https://doi.org/10.1016/j.ssi.2008.07.015.

[17] X.-L. Xia, S. Gao, Z.-G. Liu, J.-H. Ouyang, The influence of pentavalent Nb substitution for Zr on electrical properties of oxide-ion conductor $Gd_2Zr_2O_7$, Electrochim. Acta 55 (2010) 5301–5306, https://doi.org/10.1016/j.electacta.2010.04.086.

[18] F.N. Sayed, V. Grover, K. Bhattacharyya, D. Jain, A. Arya, C.G. Pillai, A.K. Tyagi, $Sm_{2-x}Dy_xZr_2O_7$ pyrochlores: probing order-disorder dynamics and multifunctionality, Inorg. Chem. 50 (2011) 2354–2365, https://doi.org/10.1021/ic2001084.

[19] T. Omata, S. Otsuka-Yao-Matsuo, S. Electrical properties of proton-conducting Ca^{2+} - doped $La_2Zr_2O_7$ with a pyrochlore-type structure, J. Electrochem. Soc. 148 (2001) E252–E261, https://doi.org/10.1149/1.1369370.

[20] T. Fournier, J.Y. Nots, J. Muller, J.C. Joubert, Conductivite ionique des phases de type pyrochlore $Gd_{2-x}Ca_xZr_2O_{7-x/2}$ et $Gd_{2-x}Ca_xSc_2O_{7-x/2}$, Solid State Ionics 15 (1985) 71–74, https://doi.org/10.1016/0167-2738(85)90110-9.

[21] F. Zhong, J. Zhao, L. Shi, Y. Xiao, G. Cai, Y. Zheng, J. Long, Alkalin-earth metals-doped pyrochlore $Gd_2Zr_2O_7$ as oxygen conductors for improved NO_2 sensing performance, Sci. Rep. 7 (2017) 4684, https://doi.org/10.1038/s41598-017-04920-1.

[22] A.V. Shlyakhtina, J.C.C. Abrantes, E. Gomes, N.V. Lyskov, E.Yu Konysheva, S. A. Chernyak, E.P. Kharitonova, O.K. Karyagina, I.V. Kolbanev, L.G. Shcherbakova, Evolution oxygen-ion and proton conductivity in Ca-doped $Ln_2Zr_2O_7$ (Ln = Sm, Gd), located near pyrochlore-fluorite phase boundary, Materials 12 (15) (2019) 2452, https://doi.org/10.3390/ma12152452.

[23] A.V. Shlyakhtina, N.V. Gorshkov, I.V. Kolbanev, K.I. Shefer, A.V. Kasyanova, D. A. Medvedev, Electrical properties of beryllium-doped $Gd_2Zr_2O_7$, Inorg. Mater. 57 (2021) 1253–1263, https://doi.org/10.31857/S0002337X21110117.

[24] Z.G. Liu, S. Gao, J.H. Ouyang, X.L. Xia, Influence of MoO_3 doping on structure and electrical conductivity of defect fluorite-type $Gd_2Zr_2O_7$, J. Alloys Compd. 506 (2010) 868–871, https://doi.org/10.1016/j.jallcom.2010.07.101.

[25] I.A. Anokhina, I.E. Animitsa, V.I. Voronin, V.B. Vykhodets, T.E. Kurennykh, N. G. Molchanova, A.I. Vylkov, A.E. Dedyukhin, Y.P. Zaikov, The structure and electrical properties of lithium doped pyrochlore $Gd_2Zr_2O_7$, Ceram. Int. 47 (2021) 1949–1961, https://doi.org/10.1016/j.ceramint.2020.09.025.

[26] I.A. Anokhina, I.E. Animitsa, A.F. Buzina, V.I. Voronin, V.B. Vykhodets, T.E. Kurennykh, Y.P. Zaikov, Synthesis, structure and electrical properties of Li+-doped pyrochlore $Gd_2Zr_2O_7$, Chimica Techno Acta. 7 (2020) 51–60.

[27] K.E.J. Eurenius, E. Ahlberg, C.S. Knee, Role of B-site ion on proton conduction in acceptor-doped $Sm_2B_2O_{7-\delta}$ (B = Ti, Sn, Zr and Ce) pyrochlores and C-type compounds, Dalton Trans. 40 (2011) 3946–3954, https://doi.org/10.1039/C0DT01347A.

[28] X.-L. Xia, J.-H. Ouyang, Z.-G. Liu, Influence of CaO on structure and electrical conductivity of pyrochlore–type $Sm_2Zr_2O_7$, J. Power Sources 189 (2009) 888–893, https://doi.org/10.1016/j.jpowsour.2008.12.136.

[29] I. Zvonareva, X.-Z. Fu, D. Medvedev, Z. Shao, Electrochemistry and energy conversion features of protonic ceramic cells with mixed ionic-electronic electrolytes, Energy Environ. Sci. 15 (2022) 439–465, https://doi.org/10.1039/D1EE03109K.

[30] Z. Qu, C. Wan, W. Pan, Thermal expansion and defect chemistry of MgO-doped $Sm_2Zr_2O_7$, Chem. Mater. 19 (2007) 4913–4918, https://doi.org/10.1021/cm071615z.

[31] X.-Z. Xiong, Z.-G. Liu, J.-H. Ouyang, X.-L. Xia, J. Xiang, X.-M. Liu, Preparation, structure and electrical conductivity of the pyrochlore-type phase Sm_2Zr_2O7 co-doped with bivalent magnesium and trivalent dysprosium cations, J. Alloys Compd. 509 (2011) 8392–8397, https://doi.org/10.1016/j.jallcom.2011.05.088.

[32] Z.-G. Liu, J.-H. Ouyang, K.-N. Sun, Y. Zhou, Influence of magnesia doping on structure and electrical conductivity of pyrochlore type $GdSmZr_2O_7$, Adv. Appl. Ceram. 111 (2013) 214–219, https://doi.org/10.1179/1743676111Y.0000000077.

[33] T. Shimura, M. Komori, H. Iwahara, Ionic conduction in pyrochlore-type oxides containing rare earth elements at high temperature, Solid State Ionics 86–88 (1996) 685, https://doi.org/10.1016/0167-2738(96)00148-8.

[34] T. Omata, K. Ikeda, R. Tokashiki, S. Otsuka-Yao-Matsuo, Proton solubility for $La_2Zr_2O_7$ with a pyrochlore structure doped with a series of alkaline-earth ions, Solid State Ionics 167 (2004) 389–397, https://doi.org/10.1016/j.ssi.2004.01.015.

[35] J.A. Labrincha, J.R. Frade, F.M.B. Marques, Protonic conduction in $La_2Zr_2O_7$-based pyrochlore materials, Solid State Ionics 99 (1997) 33–40, https://doi.org/10.1016/S0167-2738(97)00198-7.

[36] A.V. Shlyakhtina, N.V. Lyskov, E.Y. Konysheva, S.A. Chernyak, I.V. Kolbanev, G. A. Vorobieva, L.G. Shcherbakova, Gas-tight proton-conducting $Nd_{2-x}Ca_xZr_2O_{7-\delta}$ (x = 0, 0.05) ceramics, J. Solid State Electrochem. 24 (2020) 1475–1486, https://doi.org/10.1007/s10008-020-04574-6.

[37] A.V. Shlyakhtina, N.V. Lyskov, I.V. Kolbanev, G.A. Vorob'eva, A.N. Shchegolikhin, V.I. Voronkova, Specific features of phase formation and properties of compounds La2W1 + xO6 + 3x (x ~ 0; 0.11–0.22)1. ISSN 1023-1935, Russ. J. Electrochem. 59 (2023) 60–69, https://doi.org/10.1134/S1023193523010817, 2023.

[38] Impedance spectroscopy: theory, experiment, and applications, in: Evgenij Barsoukov (Ed.), Texas Instruments Inc.) and J. Ross Macdonald, University of North Carolina, Chapel Hill). John Wiley & Sons, Inc., Hoboken, NJ, 2005, p. 596, https://doi.org/10.1002/0471716243. ISBN 0471-64749-7. – 2005.

[39] R.D. Shannon, Revised effective ionic radii and systematic studies of interatomic distances in halides and chaleogenides, Acta Crystallogr. A32 (1976) 751–767, https://doi.org/10.1107/S0567739476001551.

[40] X. Vendrell, E.L. Santos-Veiga, H. Beltrán-Mir, E. Cordoncillo, L. Mestres, Induced p-type semiconductivity in Mg-doped $Nd_2Zr_2O_7$ pyrochlore system, J. Eur. Ceram. Soc. 43 (2023) 6967–6973, https://doi.org/10.1016/j.jeurceramsoc.2023.07.061.

[41] K. Shinozaki, M. Mtyauchi, K. Kuroda, O. Sakurai, N. Mizutani, M. Kato, Oxygen-ion conduction in the $Sm_2Zr_2O_7$ pyrochlore phase, J. Am. Ceram. Soc. 69 (1979) 538–539, https://doi.org/10.1111/j.1151-2916.1979.tb19131.x.

[42] A.V. Shlyakhtina, I.V. Kolbanev, E.N. Degtyarev, N.V. Lyskov, O.K. Karyagina, S. A. Chernyak, L.G. Shcherbakova, Kinetic aspects of the synthesis of $Ln_{6-x}MoO_{12-\delta}$ (Ln= Sm, Ho -Yb; x=0, 0.5) rare-earth molybdates using mechanical activation of oxides, Solid State Ionics 320 (2018) 272–282, https://doi.org/10.1016/j.ssi.2018.02.004.

[43] Klaus-Dieter Kreuer, Proton conductivity: materials and applications, Chem. Mater. 8 (1996) 610–641, https://doi.org/10.1021/cm950192a.

[44] J. Koettgen, S. Grieshammer, P. Hein, B.O.H. Grope, M. Nakayama, M. Martin, Understanding the ionic conductivity maximum in doped ceria: trapping and

blocking, Phys. Chem. Chem. Phys. 20 (2018) 14291–14321, https://doi.org/10.1039/C7CP08535D.
[45] N. Kochetova, I. Animitsa, D. Medvedev, A. Demin, P. Tsiakaras, Recent activity in the development of proton-conducting oxides for high-temperature applications, RSC Adv. 6 (2016) 73222, https://doi.org/10.1039/c6ra13347a.
[46] V. Sadykov, A. Shlyakhtina, N. Lyskov, E. Sadovskaya, S. Cherepanova, N. Eremeev, V. Skazka, V. Goncharov, E. Kharitonova, Oxygen diffusion in Mg-doped Sm and Gd zirconates with pyrochlore structure, Ionics 26 (2020) 4621–4633, https://doi.org/10.1007/s11581-020-03614-5.
[47] P. Colomban, Proton and protonic species: the hidden face of solid state chemistry. How to measure H-Content in materials? Fuel Cells 13 (2013) 6–18, https://doi.org/10.1002/fuce.2012.00088.
[48] A.V. Shlyakhtina, G.A. Vorobieva, A.N. Shchegolikhin, A.V. Leonov, I.V. Kolbanev, A.N. Streletskii, Phase relations and behavior of carbon-containing impurities in ceramics prepared from mechanically activated $Ln_2O_3 + 2HfO_2$ (ln = Nd, dy) mixtures, Inorg. Mater. 56 (2020) 528–542, https://doi.org/10.1134/S002016852005012X.